MARTIN MARIETTA

Martin Marietta Laboratories

MML TR 81-42(c)

BONDABILITY OF TI ADHERENDS

II. HUMID ENVIRONMENT EFFECTS

Prepared by

Menachem Natan
Kathleen R. Breen
John D. Venables
Martin Marietta Laboratories
1450 South Rolling Road
Baltimore, Maryland 21227

Final Report for Period 15 August 1980

through 15 September 1981

Prepared for

DEPARTMENT OF THE NAVY
Naval Air Systems Command
Washington, D.C. 20361

Baltimore DCAS Management Area
300 E. Joppa Road, Room 200
Towson, Maryland 21204
Attn: Mr. William L. Sunday, ACO

SECURITY CLASSIFICATION OF THIS PAGE *(When Data Entered)*

REPORT DOCUMENTATION PAGE

READ INSTRUCTIONS BEFORE COMPLETING FORM

1. REPORT NUMBER

2. GOVT ACCESSION NO.

3. RECIPIENT'S CATALOG NUMBER

4. TITLE *(and Subtitle)*
Bondability of Ti Adherends
II. Humid environment effects

5. TYPE OF REPORT & PERIOD COVERED
Final report (2nd year)
15-Aug.-80 - 15-Sep.-81

6. PERFORMING ORG. REPORT NUMBER
MML TR 81-42(c)

7. AUTHOR(s)
Menachem Natan
Kathleen R. Breen
John D. Venables

8. CONTRACT OR GRANT NUMBER(s)
N00019-80-C-0508

9. PERFORMING ORGANIZATION NAME AND ADDRESS
Martin Marietta Corporation
Martin Marietta Laboratories
1450 S. Rolling Road
Baltimore, Maryland 21227-3898

10. PROGRAM ELEMENT, PROJECT, TASK AREA & WORK UNIT NUMBERS

11. CONTROLLING OFFICE NAME AND ADDRESS
Department of the Navy
Naval Air Systems Command
Code: AIR - 5304C2
Washington, D.C. 20361

12. REPORT DATE
September 22, 1981

13. NUMBER OF PAGES
54

14. MONITORING AGENCY NAME & ADDRESS *(if different from Controlling Office)*
Baltimore DCAS Management Area
300 E. Joppa Road, Room #200
Towson, Maryland 21204
Attention: Mr. William L. Sunday, ACO

15. SECURITY CLASS. *(of this report)*
Unclassified

15a. DECLASSIFICATION/DOWNGRADING SCHEDULE

16. DISTRIBUTION STATEMENT *(of this Report)*
Approved for public release; distribution unlimited.

17. DISTRIBUTION STATEMENT *(of the abstract entered in Block 20, if different from Report)*
N/A

18. SUPPLEMENTARY NOTES

19. KEY WORDS *(Continue on reverse side if necessary and identify by block number)*
titanium, adhesive bonding, surface treatments, oxide morphology, oxide crystal structure, amorphous TiO_2-anatase transformation, STEM, TEM, SAD, water immersion effects, oxide dissolution, oxide precipitation, bond durability

20. ABSTRACT *(Continue on reverse side if necessary and identify by block number)*
Over

DD FORM 1 JAN 73 1473

SECURITY CLASSIFICATION OF THIS PAGE *(When Data Entered)*

Abstract

We have demonstrated the importance of oxide morphology to the properties of bondments of Al and Ti structures in previous studies. Microrough, porous oxides which provide good mechanical interlocking with the primer/adhesive system were found essential to good bondability. Ability to withstand long-term degradation in humid environments in Al was found to be poor, because the Al oxide was transformed into hydroxide in a relatively short time. On the other hand, Ti oxides are known to be very stable. The purpose of this study was to investigate possible humidity-induced morphological and structural changes on these latter oxides and to relate them to known failure data. We found that both changes occur at temperatures/times relevant to service conditions. Typically, the original oxides are amorphous TiO_2. They crystallize into anatase through a dissolution-precipitation process, which is strongly dependent on temperature, oxide porosity and surface contamination. This transformation may be important in the degradation of adhesive bonds to Ti.

MML TR 81-42(c)

BONDABILITY OF TI ADHERENDS

II. HUMID ENVIRONMENT EFFECTS

Prepared by

Menachem Natan
Kathleen R. Breen
John D. Venables
Martin Marietta Laboratories
1450 South Rolling Road
Baltimore, Maryland 21227

Final Report for Period 15 August 1980 - 15 September 1981

Prepared for

DEPARTMENT OF THE NAVY
Naval Air Systems Command
Washington, D.C. 20361

Principal Investigator: M. Natan
M. Natan

Co-Principal Investigator: Kathleen Ruth Breen
K. R. Breen

Co-Principal Investigator: John D. Venables
J.D. Venables

TABLE OF CONTENTS

LIST OF FIGURES

LIST OF FIGURES (Continued)

I. INTRODUCTION

The bondability of Ti adherends has been shown in prior work on this program[1] to depend primarily on the oxide morphology of the adherends and only secondarily on the composition of the surface oxide. Various treatment processes for preparing Ti for adhesive bonding produce oxide morphologies that could be placed into three groups according to the microroughness of the oxide. Thick porous oxides, e.g., those on chromic-acid-anodized (CAA) surfaces, provide the best bondability as determined by wedge tests and stress-durability measurements. In contrast, smooth, non-porous oxides, as on phosphate-fluoride (PF) treated surfaces, provide poor bondability. In the latter case, the major contribution to interfacial strength comes from chemical bonds between adhesive and oxide rather than mechanical interlocking provided by porous oxides.

In our initial work, morphology characterization studies were greatly advanced by the introduction of high resolution scanning electron microscopy employing a STEM. In this study, we have extended the use of this technique to study morphology changes induced by humidity. Such changes, occurring on Ti adherends in humid environments, have been little studied in the past, probably due to the well-deserved reputation of Ti as an extremely corrosion-resistant material. As the following short literature survey proves, very little firm data in regard to adherend oxide morphology and structure were available as a starting point. Therefore, a major part of this study is dedicated to getting a basic understanding of these subjects and their relevance to humidity exposure effects.

---

1 B.M. Ditchek, K.R. Breen, T.S. Sun, J.D. Venables and S.R. Brown, 12th Nat. SAMPE Tech. Conf., Seattle, WA (1980), p. 882.

Past studies dealt with oxide formation on Ti surfaces by corrosion[2] and by chemical conversion and anodization.[3-12] The latter generally produce oxides having a TiO_2 composition,[3,4,5] although $TiO_2 + TiF_4$,[6] and $TiO_2 + Ti_2O_3$[7] are also mentioned. Deviations from the TiO_2 stoichiometry do occur, as shown by the variation in peak-height of the two elements under Auger examination.[1,6] TiO_2 was described as crystalline[3,5,8,9,10] or amorphous.[5,8,9,11,12] In its crystalline form it may appear as one of three polymorphs: brookite, anatase, and rutile. Although brookite and anatase are "metastable" under normal conditions, their solid state transformation into rutile -- the stable form -- is extremely slow below ca. 600°C. Anatase and rutile are the most often mentioned structures on Ti-6Al-4V adherends: anatase on PF,[3,5] VAST/H_2SiF_6,[5] and H_2SO_4-anodized surfaces,[9] and rutile on Pasa Jell 107,[5] Turco 5578,[5] alkaline hydrogen peroxide,[10] and high voltage H_2SO_4-anodized[9] surfaces. Amorphous or mixtures of amorphous and crystalline structures were found on Ti surfaces treated by: PF,[8,12] amorphous; low voltage H_2SO_4 anodization,[9] amorphous + anatase; and Pasa Jell 107,[5] amorphous + rutile. Amorphous TiO_2 was also found on Ti films prepared in a phosphoboric bath at pH 1.[11]

There are very few reports of structural and chemical changes in the Ti adherend oxides exposed to humidity, except for the often mentioned conversion of anatase to rutile.[3] In view of this, the need for more research in the subject is evident. It is especially important to determine

---

2 A.C. Fraker and A.W. Ruff, Jr., Corros. Sci. 11 (1971), 763-5.
3 W.C. Hamilton, G.A. Lyerly and J. Fronhsdorf, Technical Report 4362, 6/1972, Gillette Research Institute, Rockville, MD.
4 A.A. Roche, Technical Report AFWAL-TR-80-4004, Feb. 1980.
5 G.W. Lively, Technical Report AFML-TR-73-270, Jan. 1974.
6 A.A. Roche, J.S. Solomon and W.L. Baun, Appl. Surf. Sci. 7 (1981), 83-96.
7 J.M. Abd El Kader, F.M. Abd El Wahad, H.A. El Shayeb and M.G.A. Khedr, Br. Corros. J. 16(2) (1981), 111-114.
8 F. Dalard, C. Montella and J. Gandon, Surf. Technol. 8 (1979), 203-224.
9 G. Blondeau, M. Froelicher, M. Froment and A. Hugot-LeGoff, Proc. 7th Int. Vac. Congr. and 3rd Int. Conf. Solid Surf., Vienna (1977), 1789-1791.
10 K.W. Allen, H.S. Alsalim and W.C. Wake, J. Adhes. 6 (1974), 153-164.
11 A. Polity, G. Jouve and P. Lacombe, J. Less-Common Met. 56 (1977), 263-268.
12 T. Smith and D.H. Kaelbe, Technical Report AFML-TR-74-73, June 1974.

the nature of the initial oxide, i.e., whether it is amorphous or crystalline. Thermodynamic arguments have been used to show that amorphous films are always metastable in comparison to their stable crystalline counterparts,[13] and this contention is apparently supported by the behavior of aluminum adherends in water. Amorphous Al_2O_3 films react almost instantaneously with water to yield a "cornflake" hydroxide[14] whereas pure sapphire exhibits great stability in boiling water, with surface morphology unchanged in periods up to one week.[15] It is also known that upon exposure to hydrothermal conditions in water, structural changes in TiO_2 follow the sequence:[16] amorphous titanium dioxide → anatase → rutile. Therefore, efforts to improve bondability through increased structural oxide stability must, of necessity, start with a complete characterization of the oxide.

This study continues along the general lines of our previous work[17] and is concerned with:

1) Characterization of the morphology of Ti adherends not included in the previous work.

2) An in-depth look at morphological and structural changes in adherend surfaces exposed to humidity, using sophisticated surface techniques including high resolution STEM, electron diffraction, and Auger/ESCA.

3) Suggestions for development of improved adherend surfaces.

---

13 K.H. Behrndt, J. Vac. Sci. Technol. 7(3) (1969), 385-398.
14 J.D. Venables, D.K. McNamara, J.M. Chen, B.M. Ditchek, T.I. Morgenthaler, T.S. Sun and R.L. Hopping, 12th Nat. SAMPE Tech. Conf., Seattle, WA, (1980), p. 909.
15 J.S. Ahearn, private communication.
16 A. Matthews, Am. Mineral. 61 (1976), 419-424.
17 B.M. Ditchek, K.R. Breen and J.D. Venables, MML TR-80-17c, Final Report to NAVAIRSYSCOM, Contract #N00019-79-C-0294 (1980).

II. EXPERIMENTAL

A. Ti ADHERENDS

The following adherends were used in this study and are identified by code in Appendix A:

a) Characterization: VA-7, PF-3, and AP-9

b) Immersion studies: TU-8, AP-9, CAA, and PF. The latter two were prepared at Martin Marietta Laboratories, according to the processes described in Appendix A.

B. WATER IMMERSION

Four specimens approximately 1 cm^2 in area were cut from coupons of each of the following adherends: PF, TU-8, CAA, and AP-9. The specimens were ultrasonically cleaned in electronic grade ethanol and placed in individual glass tubes filled with hot, deionized distilled water. The tubes were plugged with glass stopcocks and set in a Fisher Isotemp Dry Bath held at 85°C. At intervals of 25, 50, 75, and 210 hours, one specimen from each group was removed from its tube and dried in hot air. Samples from each exposure period were set aside for high resolution SEM and electron diffraction. The effect of temperature on the rate of oxide transformation was checked by immersing CAA samples in distilled water at 80°C in a humidity chamber and at 140°C in a Parr bomb. Two runs were made to check the effect of salt water on a CAA surface at 85°C and 140°C.

C. SURFACE MORPHOLOGY STUDIES

Specimen surfaces were examined by high resolution SEM in a JEOL 100-CX STEM. Charging effects by the electron beam were reduced by coating the specimens with an extremely thin layer of Pt by secondary ion deposition.

Stereo pairs of the surface were obtained on a split screen CRT using a 6° tilt angle, with accelerating voltages of 40 kV.

D. CRYSTAL STRUCTURE STUDIES

The structure of the oxides on various Ti adherends was investigated with the electron diffraction mode in the JEOL 100-CX STEM, at 100 kV. Bright- and dark-field images from selected areas were correlated with SAD (selected area diffraction) patterns. Thin foils for TEM were prepared from bulk adherends without oxide stripping, as detailed below:

Small (0.5 cm^2) samples were cut from adherend coupons or from specimens previously exposed to water and were glued to stainless steel blocks with an acetone soluble, low temperature adhesive (Crystalbond 509*). Each sample was mechanically thinned to 50-100 μm by polishing on a succession of SiC papers. The oxide was protected from damage and contamination by the glue. After polishing, the sample was removed from the block and cleaned by ultrasonic agitation in electronic grade acetone. Discs 3 mm in diameter were punched out with a small precision die, coated on the oxide side with FORMVAR, and mounted in a special holder for ion milling. Milling was done in a Technics unit with an argon ion beam impacting the rotating disc at a 17-degree angle to the base (Ti side). Typical milling conditions were 5 kV, 10 μA ion current, 1 mA gun current, and 1-5 days. Disc temperature due to ion impact was estimated as no higher than 100°C and was not expected to affect the oxide structure. The FORMVAR protected the surface against backstreaming oil contamination and was removed after milling by soaking the disc in ethylene dichloride for 1 hour. Milling stopped automatically after a breakthrough occurred in the disc. The edges of the hole thus obtained contained enough thin areas to permit transmission viewing. Some of the thin areas contained only oxide; others showed the presence of the Ti substrate. In the discussion of our results, we show that the ion beam caused no significant damage to the observed structures.

---

* Aremco Products Inc.

III. RESULTS AND DISCUSSION

A. ADHEREND CHARACTERIZATION

1. VA-7

In the VA-7 process, the Ti surface is blasted with a 2% H_2SiF_6/Al_2O_3 slurry, a treatment that both etches and abrades the surface. Figure 1 shows an electron micrograph collage of the treated adherend. It is highly deformed, with morphology similar to that developed in the PF process, and can be assigned to Group I due to its lack of sharp macrorough detail and lack of microroughness (Figure 2a). Bond strength and durability are therefore expected to be low, similar to those of PF. ESCA analysis of the surface indicated Si and Al contamination, probably from the slurry, but no F.

2. AP-9

The morphology of an AP-9-treated Ti adherend is shown in Figure 3. Its fine porosity, characteristic of Group III surfaces, should provide a mechanical component to bond strength. However, compared to the other adherend surface in this group -- CAA -- the AP-9 adherend is less porous and may not provide as strong or durable a bond. Auger analysis and depth profiling data are presented in Figures 4 and 5. No significant contamination, e.g., F, was found on this surface, and the oxide thickness as indicated by the depth profiling is 550-600 Å. We should mention that this adherend oxide is only half as thick as the one prepared at Martin Marietta Laboratories and significantly less porous. Studies to determine the reason for differences observed between laboratory- and production-prepared AP surfaces will be performed in the third year of this contract.

Figure 1. A collage of electron micrographs showing the surface of a VA-7 adherend.

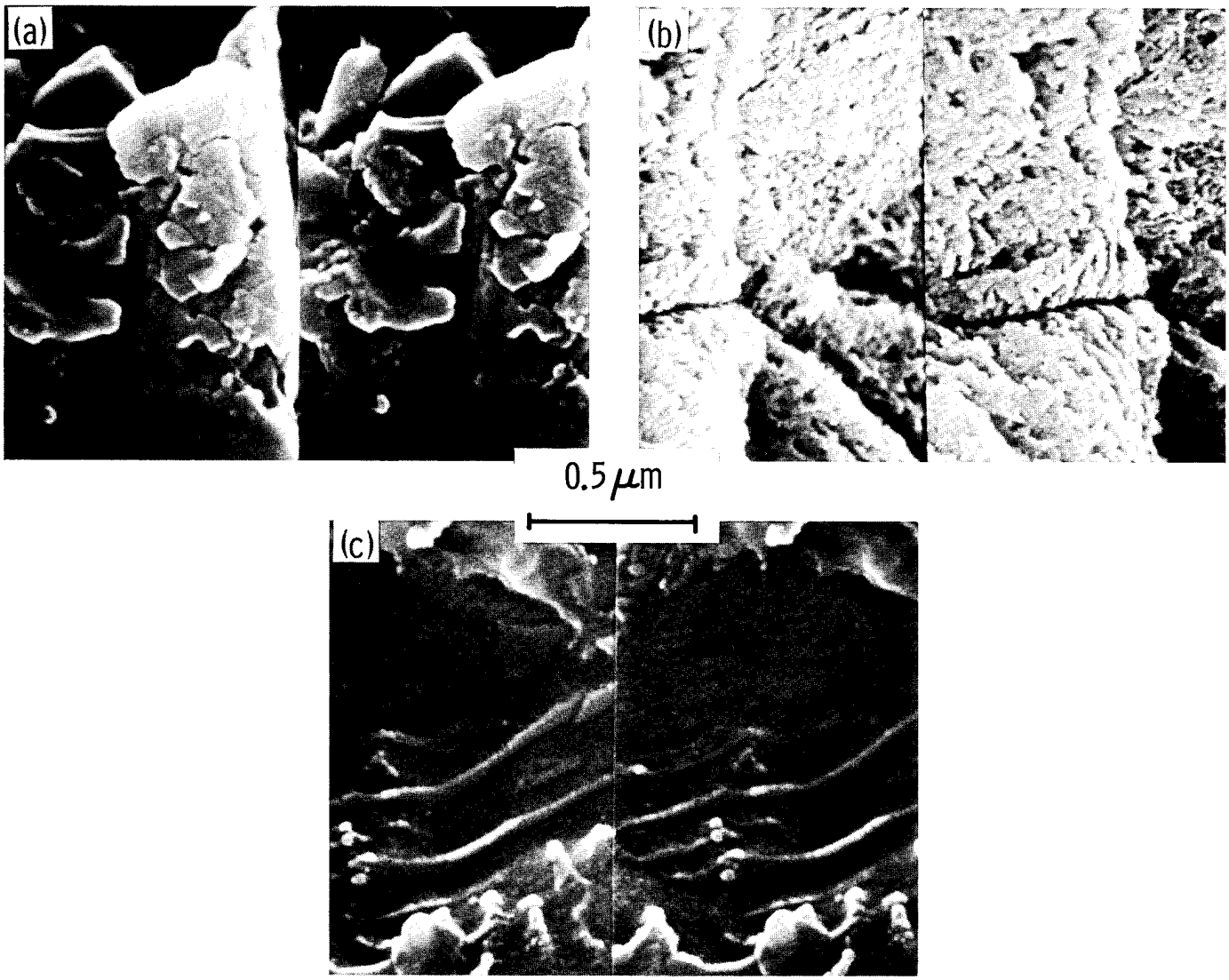

Figure 2. Stereo electron micrographs of (a) VA-7, (b) AP-9, and (c) PF-3 at high magnification.

Figure 3. A collage of electron micrographs showing the surface of an AP-9 adherend.

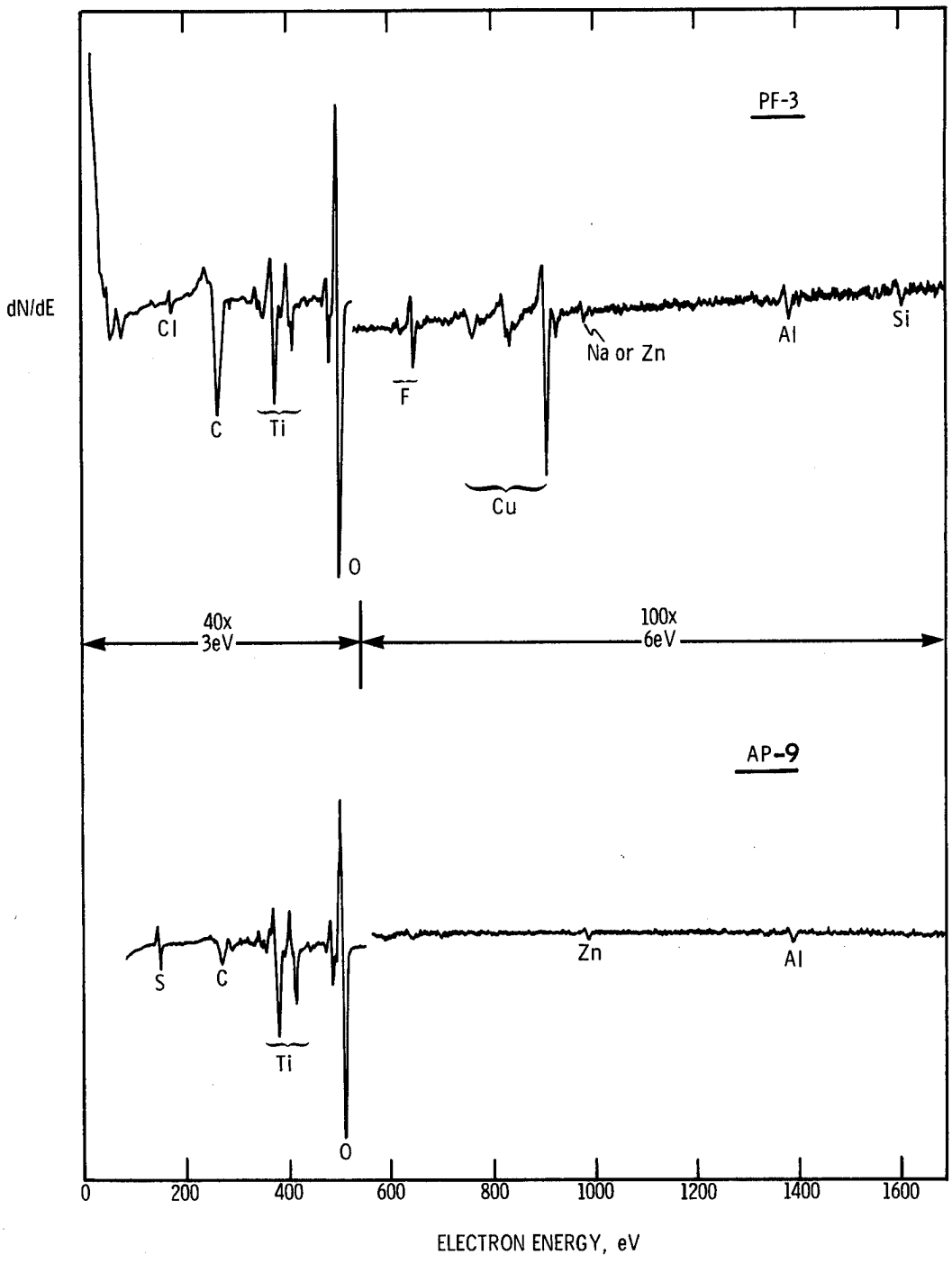

Figure 4. Auger spectra of the PF-3 and AP-9 adherends. Note the substantial copper contamination on the PF-3 surface. (Lock-in amplifier sensitivity; 40X, 100X; Modulation voltage: 3eV, 6eV.)

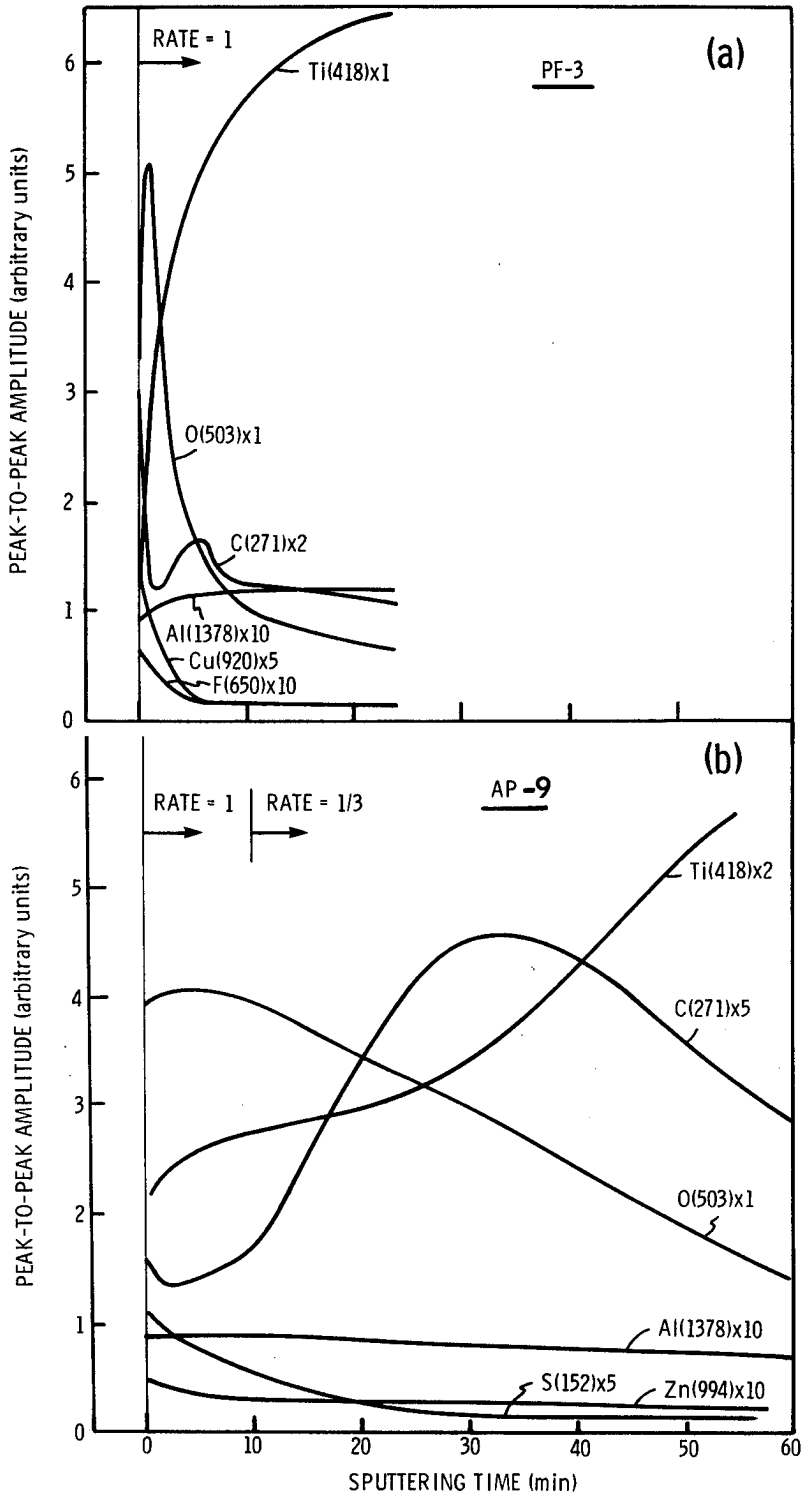

Figure 5. Auger depth profiles of the oxide on (a) the PF-3 adherend and (b) the AP-9 adherend. Sputtering rate 30Å/min.

3. PF-3

We expected this pretreatment to form a surface oxide similar to those of other PF processes. A collage of SEM pictures (Figure 6) shows that the morphology is indeed similar, with minor differences. The stereo pair in Figure 2c shows that PF-3 does not exhibit ridge formation, as does PF-1, and its oxide is microscopically rough to a lesser degree than that of PF-4. This morphology should place PF-3 in Group I; therefore bondability would be expected to be inferior to that of porous surfaces, such as CAA. Energy dispersive analysis performed in the STEM showed no surface contamination, but Auger analysis (Figure 4) and depth profiling (Figure 5) showed a significant amount of copper on the oxide surface. This contaminant disappears as the oxide is sputtered away, leading us to believe that a processing step, maybe the bath itself, might have caused the top oxide layer copper enrichment. Smith and Kaelbe[12] also found copper on PF surfaces, but in lower concentrations.

B. HOT WATER IMMERSION EFFECTS ON Ti ADHERENDS

The four types of adherends used in this experiment, chosen to represent each of the morphology groups, were: PF (Group I); TU-8 (Group II); CAA (Group III); and the alkaline peroxide specimen, AP-9, which we assigned to Group III. The morphological differences of the original adherends prior to water immersion were detailed in the first part of this project.[17] In addition, there are variations in structure, acidity and contaminants. Ti-6Al-4V consists of two phases -- α, which is Al-rich and has an hcp structure, and β, which is vanadium rich and has a bcc structure. The PF treatment etches the α phase preferentially, leaving a relief primarily of the β phase.[10] The thin oxide (100 Å) is contaminated with F.[17] The TU-8 surface has no clear α-β separation and has a pH of 7.3-9.2.[18] It

---

18 R. Siriwardane and J.P. Wightman, Final Report NASA-CR-162903, March 1980.

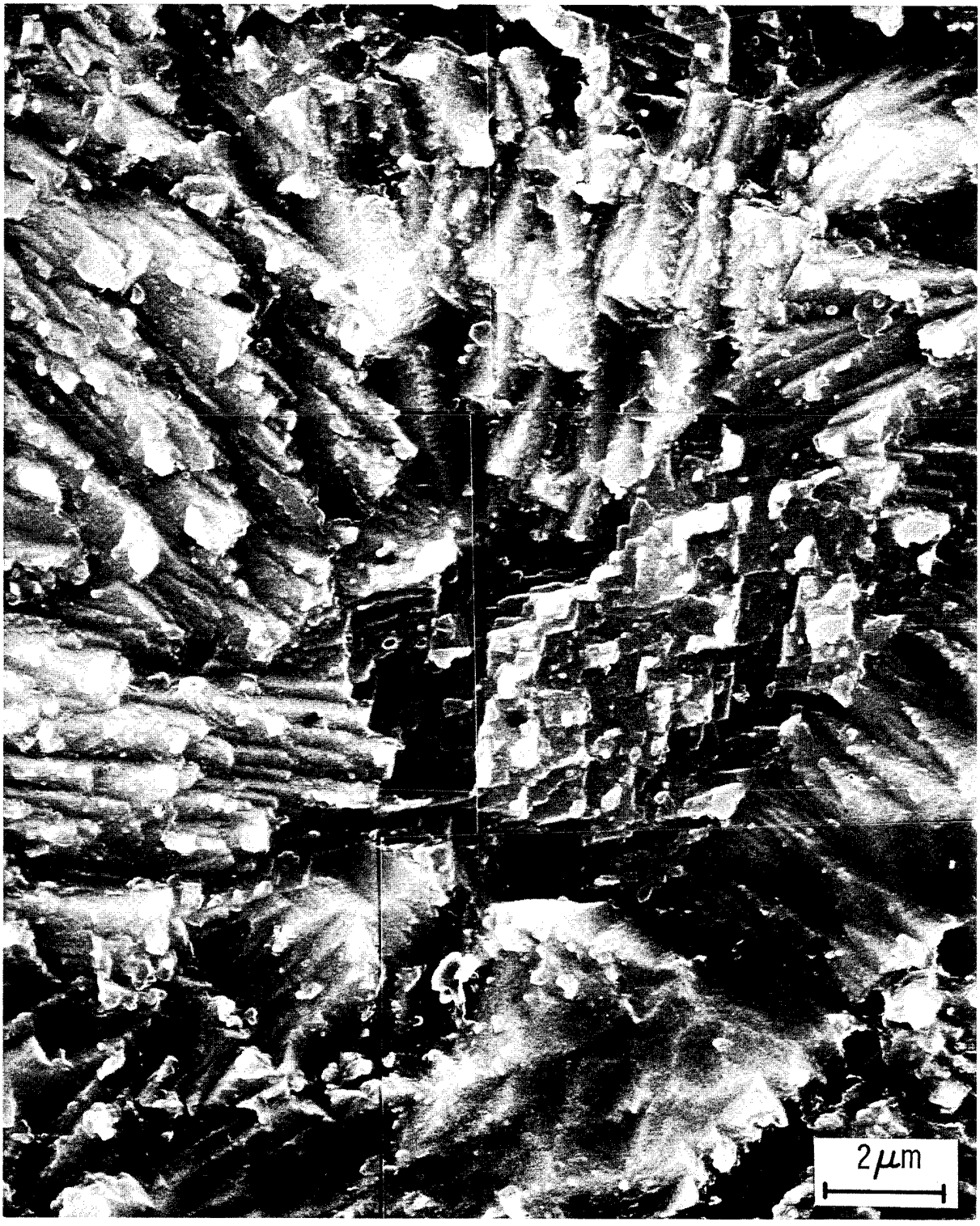

Figure 6. A collage of electron micrographs showing the surface of a PF-3 adherend.

has an oxide thickness of 175 Å(17) and is contaminated with Fe particles. The CAA surface prepared at Martin Marietta Laboratories is covered with a thick, porous, cellular oxide and has about 6% of a monolayer of F contamination. The AP surface is extremely sensitive to the peroxide bath composition.(17) Ours has a thick oxide, and we will assume that it is basic because of the forming bath. It shows no significant contamination when checked with Auger electron spectroscopy.

All four surfaces are shown in stereo electron micrographs at relatively low (10K) magnification in Figure 7, (a) prior to water immersion, and (b) after 210 hours in 85°C water. The areas chosen are typical. Within 210 hours, morphology changes occur on all four adherends, the most dramatic on the CAA surface. The crystal structure of the oxides also changes, from what originally is essentially amorphous TiO_2 (an approximate Ti/O peak ratio of 0.5 can be derived from Figure 4) to a layer of anatase crystallites covering the surface. At 210 hours, this coverage is total and uniform on the TU-8, CAA, and AP-9 surfaces, but is only about 80% of the PF surface. The anatase crystallites are approximately equidimensional, with a diameter of 100-500 Å on the PF, TU-8, and AP-9 surfaces, and elongated as "spikes" on the CAA, although such spikes were also found in small numbers on the other three. The maximum spike length on the CAA surface is on the order of 2,500 Å, comparable to the crystallite size observed by Fraker and Ruff in saline water corrosion studies of Ti alloys.(20) More details are shown in the high magnification SEM stereo pairs, the TEM micrographs of bright- and dark-field images, and the SAD patterns (Figures 8 through 17). The complex water-oxide reaction is described for each separate adherend in the following paragraphs.

---

19 W. Chen, D.W. Dwight and J.P. Wightman, Symposium on Surface Analysis, Pittsburgh Conf. on Analytical Chem. and Appl. Spectrosc., Cleveland, OH, May 12-16, 1978.

20 A.C. Fraker and A.W. Ruff, Titanium Sci. Tech., Vol. 4, Proc. Int. Conf., 2nd (1973), 2655-63.

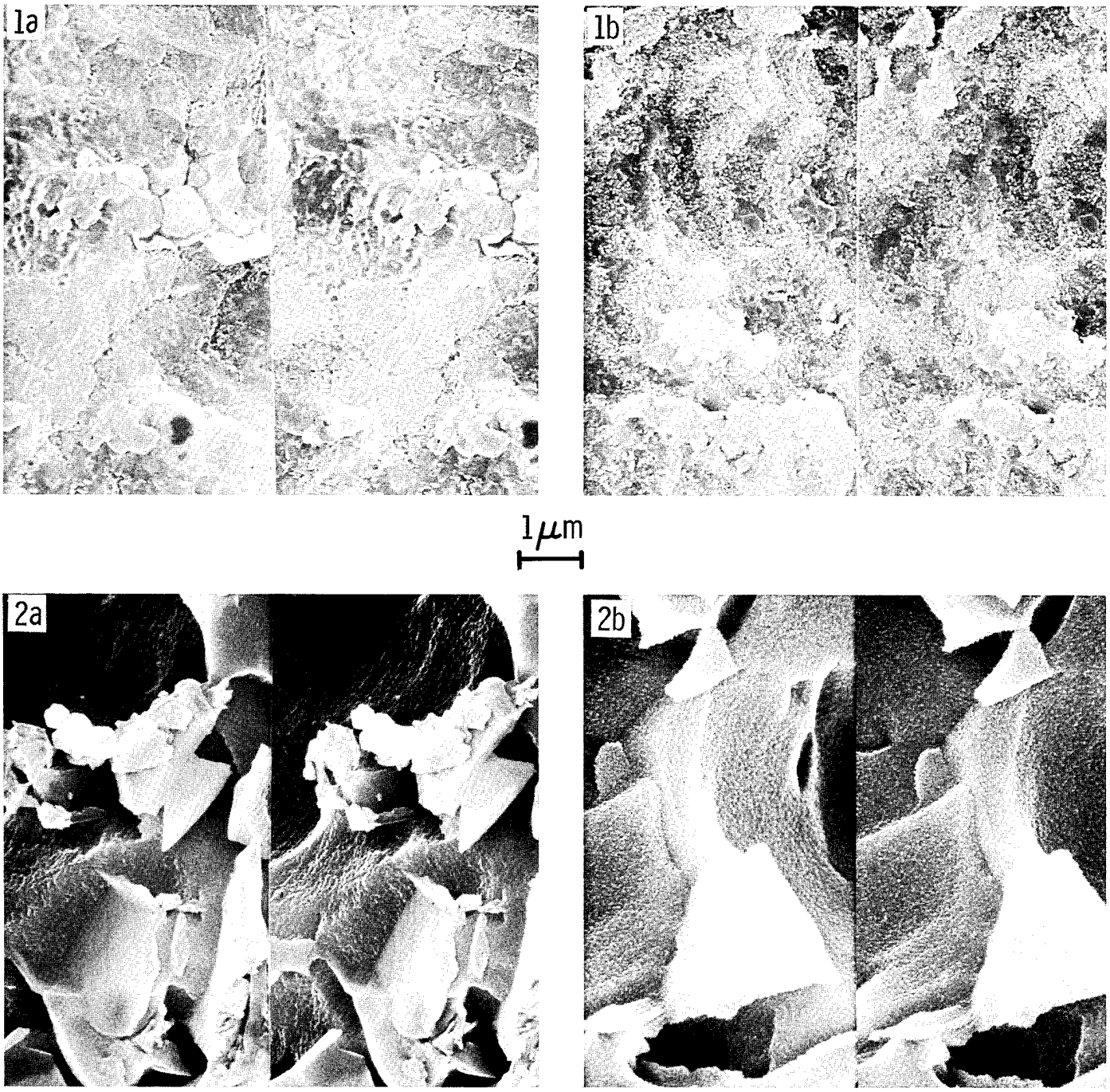

Figure 7. Stereo electron micrographs of various Ti-6Al-4V adherends (a) before and (b) after immersion in 85°C water for 210 hours. Surface treatments were: (1) phosphate fluoride, (2) Turco 5578, (3) chromic acid anodization and (4) alkaline peroxide.

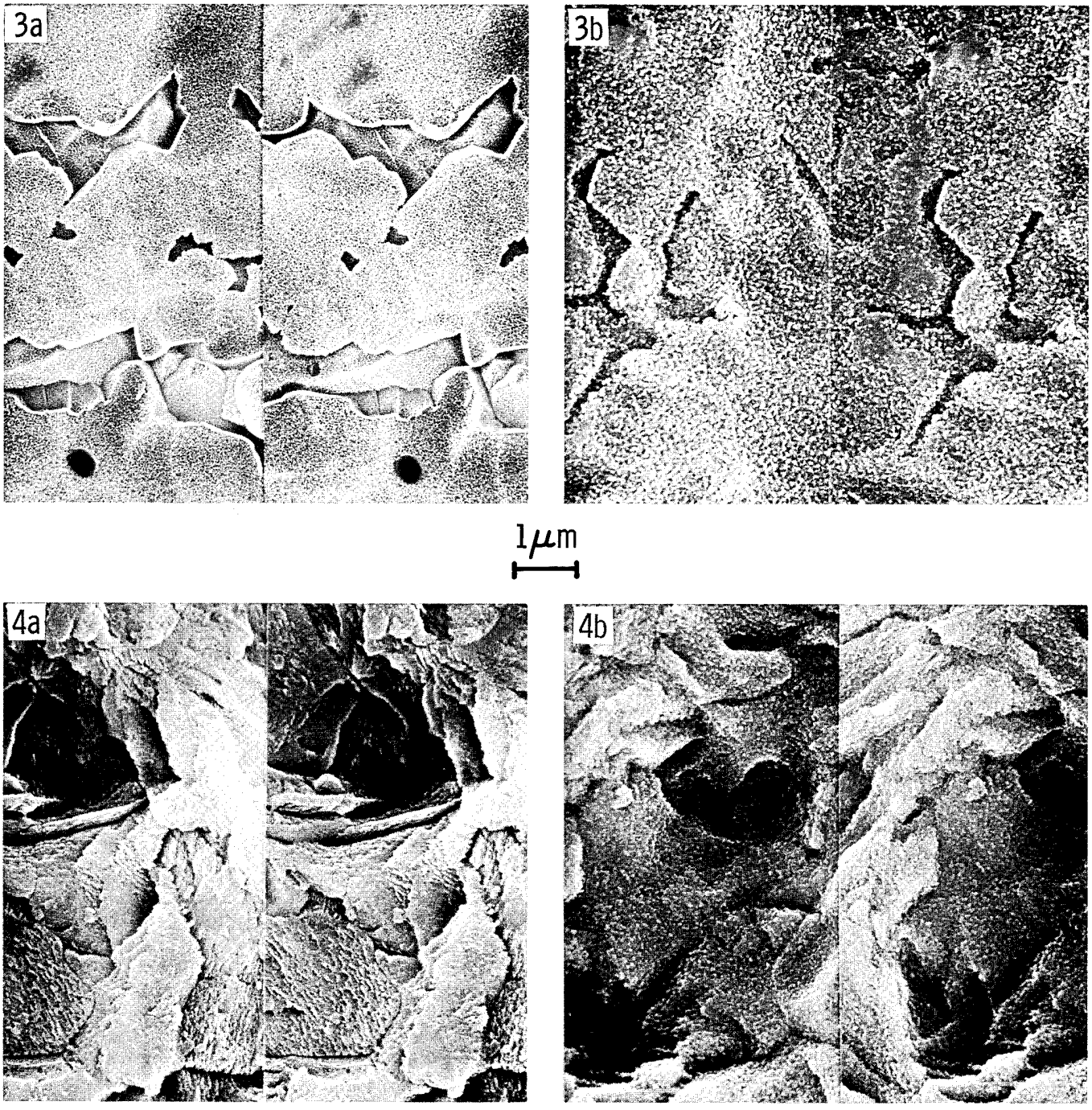

Figure 7. Continued

1. PF

The progressive morphology change at different immersion times is shown in Figure 8. The oxide on the as-prepared surface is non-porous, and, as seen in the TEM micrograph in Figure 9, quite uniform. Selected area diffraction from the region in Figure 9a shows a polycrystalline ring pattern which is unmistakenly cubic TiO (Appendix B, Table I). Dark-field imaging (not shown) indicates that the pattern comes from small crystallites dispersed in the oxide. The two broad diffuse bands in the pattern prove that the rest of the oxide film is amorphous. The significance of the presence of cubic TiO crystallites is unknown, although it is possible that they provide nucleation sites for growth of a new phase as observed below.

The new phase, consisting of small equidimensional crystallites is already present at 25 hours (Figure 8b); its incubation time, therefore, is less than 25 hours at 85°C. Crystallite size increases only slightly after 50 hours (Figure 8c) and slightly more after 210 hours (Figure 8d). Their shape remains equidimensional and polygonal, although in some areas elongated spikes, about 1000-Å long, were observed. In transmission electron micrographs (Figure 10), small crystallites, about 100-500 Å in diameter, are seen dispersed in the oxide layer. The diffraction pattern identifies them as anatase. The match in crystallite size between SEM and TEM micrographs is excellent, indicating that the ion milling technique used in TEM sample preparation causes no major structural damage. Some adherend surface "patches" remain clear of anatase even after 210 hours.

Possible oxide transformation mechanisms and the influence of other factors, such as surface acidity, will be presented in a later section.

2. TU-8

The changes in morphology on the TU-8 surface differ from those on PF in one main respect: The anatase crystallites on TU-8 are uniformly dispersed over the entire surface at all times (Figure 11). Otherwise, crystallite size (100-500 Å), shape, and incubation time are similar. A transmission

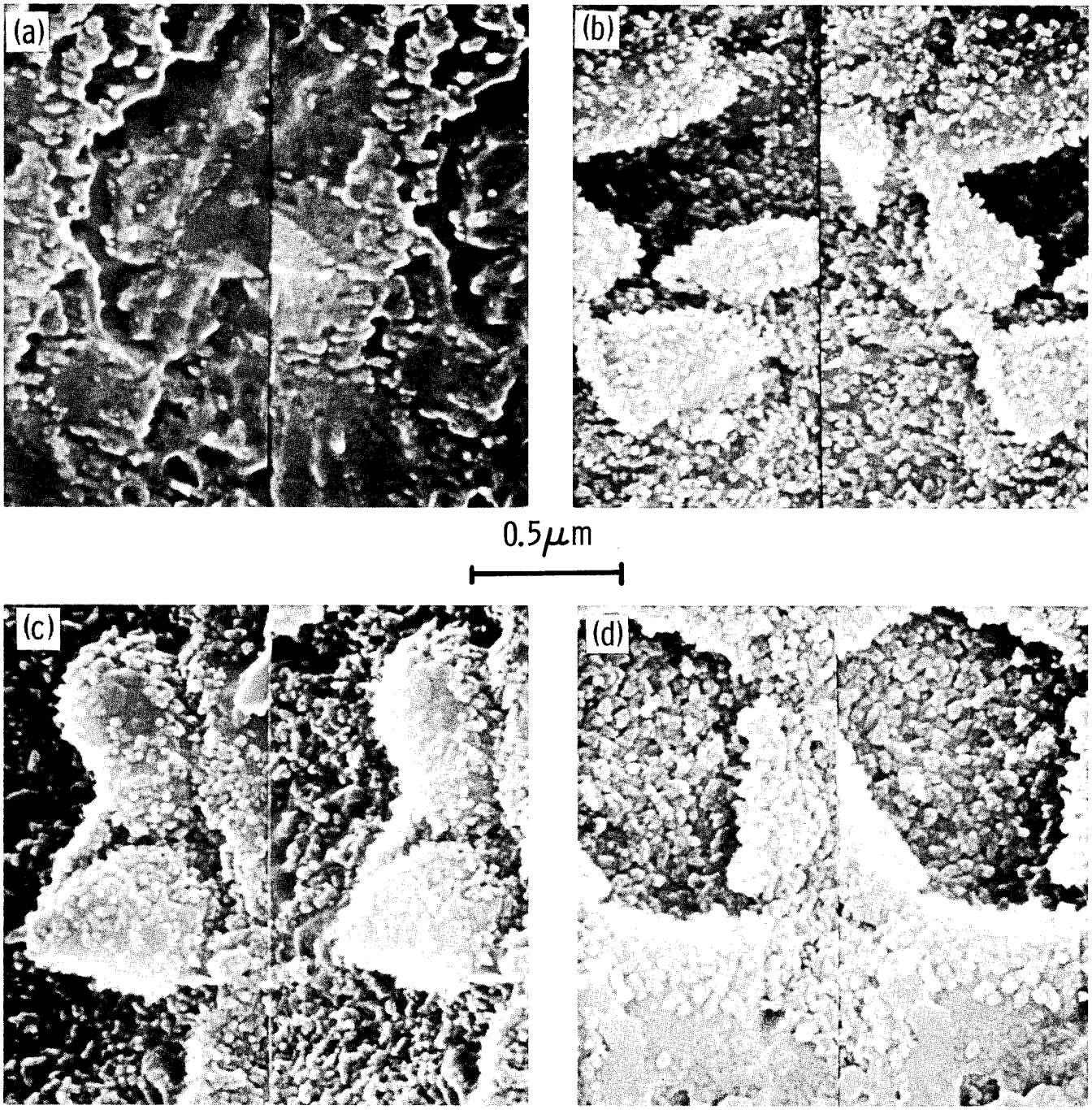

Figure 8. Stereo electron micrographs of surfaces of PF-treated Ti-6Al-4V after immersion in 85°C water for (a) 0, (b) 25, (c) 50, and (d) 210 hours.

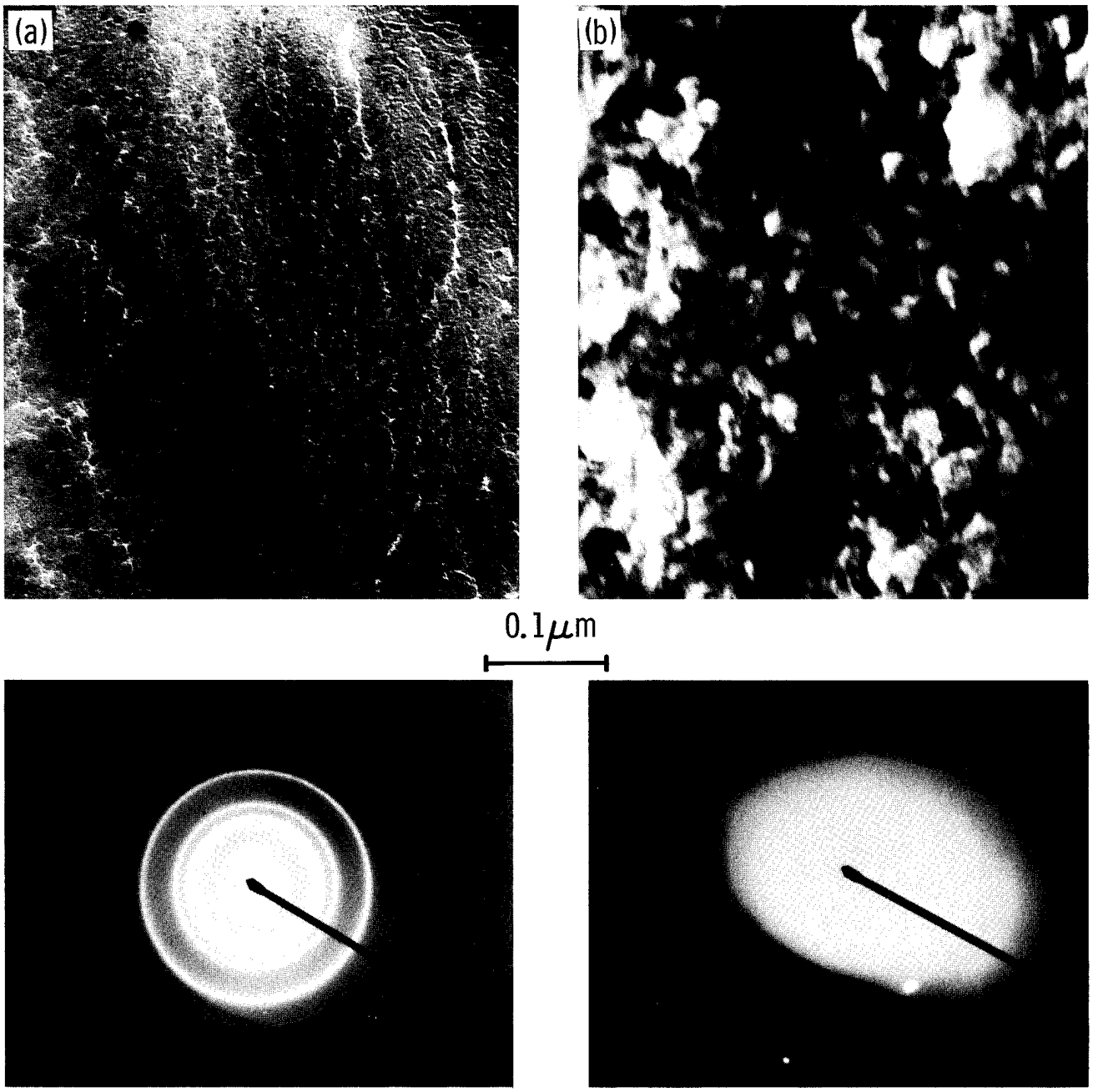

Figure 9. Transmission electron micrographs of a) the PF and b) the TU-8 oxides prior to water immersion. The SAD pattern for PF is that of crystalline cubic TiO. The TU-8 oxide is totally amorphous.

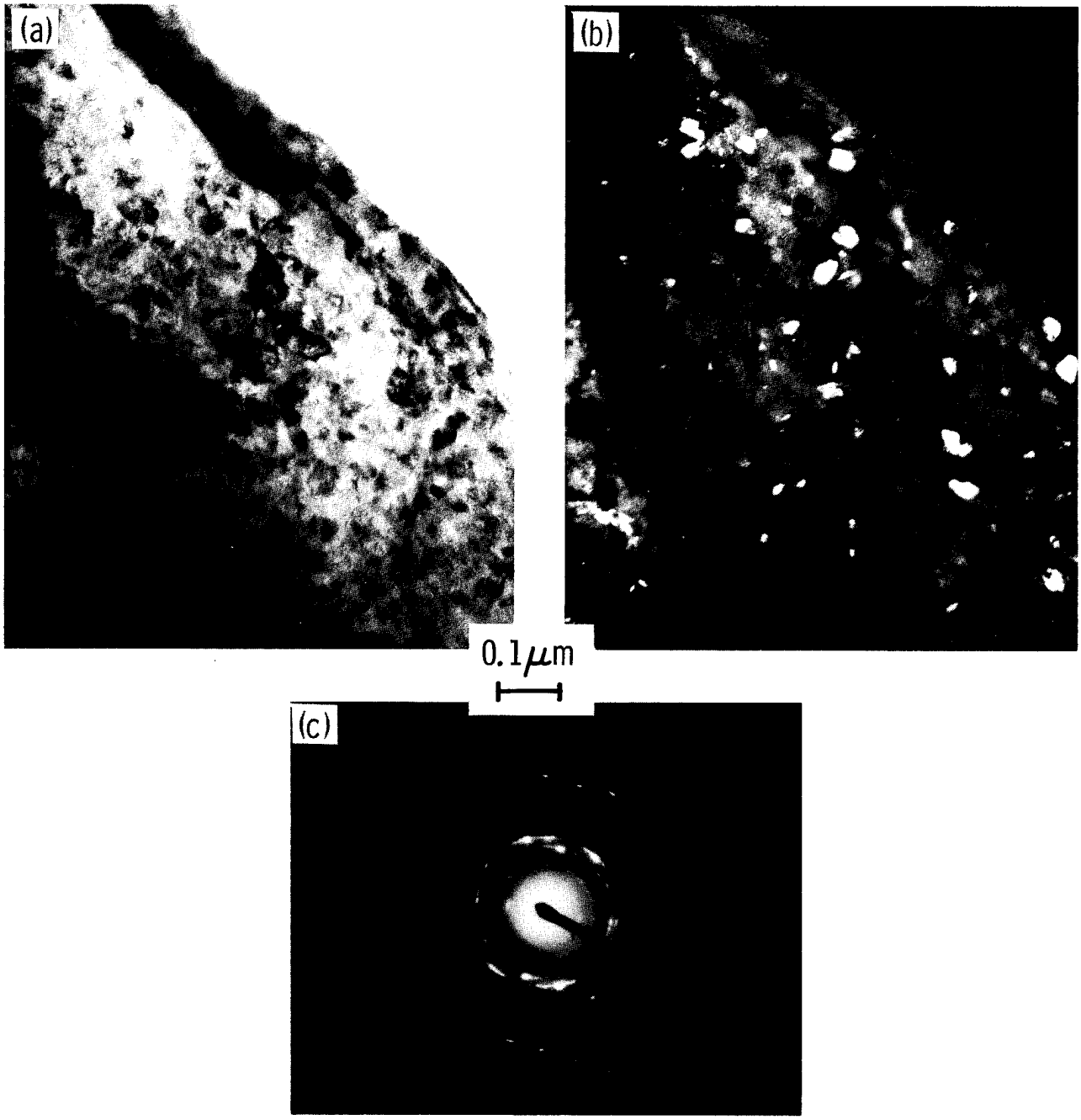

Figure 10. Transmission electron micrographs from the PF oxide after immersion for 210 hours in 85°C water: a) Bright field, b) Dark field, and c) SAD pattern. The dark-field image was taken from the {101} anatase reflection (innermost ring).

micrograph of the TU-8 oxide and its accompanying SAD pattern (Fig. 9b) shows that it is nonporous and totally amorphous, a result quite different from that in Ref. (5). Selected area diffraction of some other areas in the thin edge of the transmission specimen show a faint ring pattern, which could be that of cubic TiO, but which is definitely less developed than that on PF. In view of the proven similarity of crystallite features in TEM and SEM, it is unlikely that this structural difference (and others shown later) are an artifact induced by ion beam milling. We conclude that the PF oxide contains a better developed cubic TiO phase than the TU-8 oxide.

The TU-8 oxide is thicker than the PF oxide, and the surface is basic(18) and has no F contamination. Particles of Fe are seen on the sur face by SEM/EDS. Although the more uniform anatase distribution may be influenced by one or more of these factors, some of them are clearly less important than others. Surface acidity may influence anatase formation by affecting the solution pH. As solutions become basic, anatase formation should be inhibited.(20) However, the anatase coverage on the TU-8 surface is more uniform than on PF, indicating that this factor is unimportant. The presence of Fe on the surface may enrich the Fe ion content of the solution, which in turn may increase the probability of rutile rather than anatase formation.(21) This does not seem to happen either. It appears then that the shared characteristics of both oxides -- both being relatively thin, smooth, and nonporous -- have a greater effect on the oxide phase transformation than their differences. Our TEM micrographs (Figure 12 a,b) confirm the morphology observations and the SAD pattern (Figure 12c) is indexed as anatase. The pattern exhibits a much stronger {101} anatase reflection when compared with those of other immersed adherends.

3. AP-9

The change in morphology upon water immersion of this adherend is shown in Figure 13. The original oxide is thick, totally amorphous, and

---

21 F. Izumi and Y. Fujiki, Bull. Chem. Soc. Japan 69(3) (1976), 709-712.

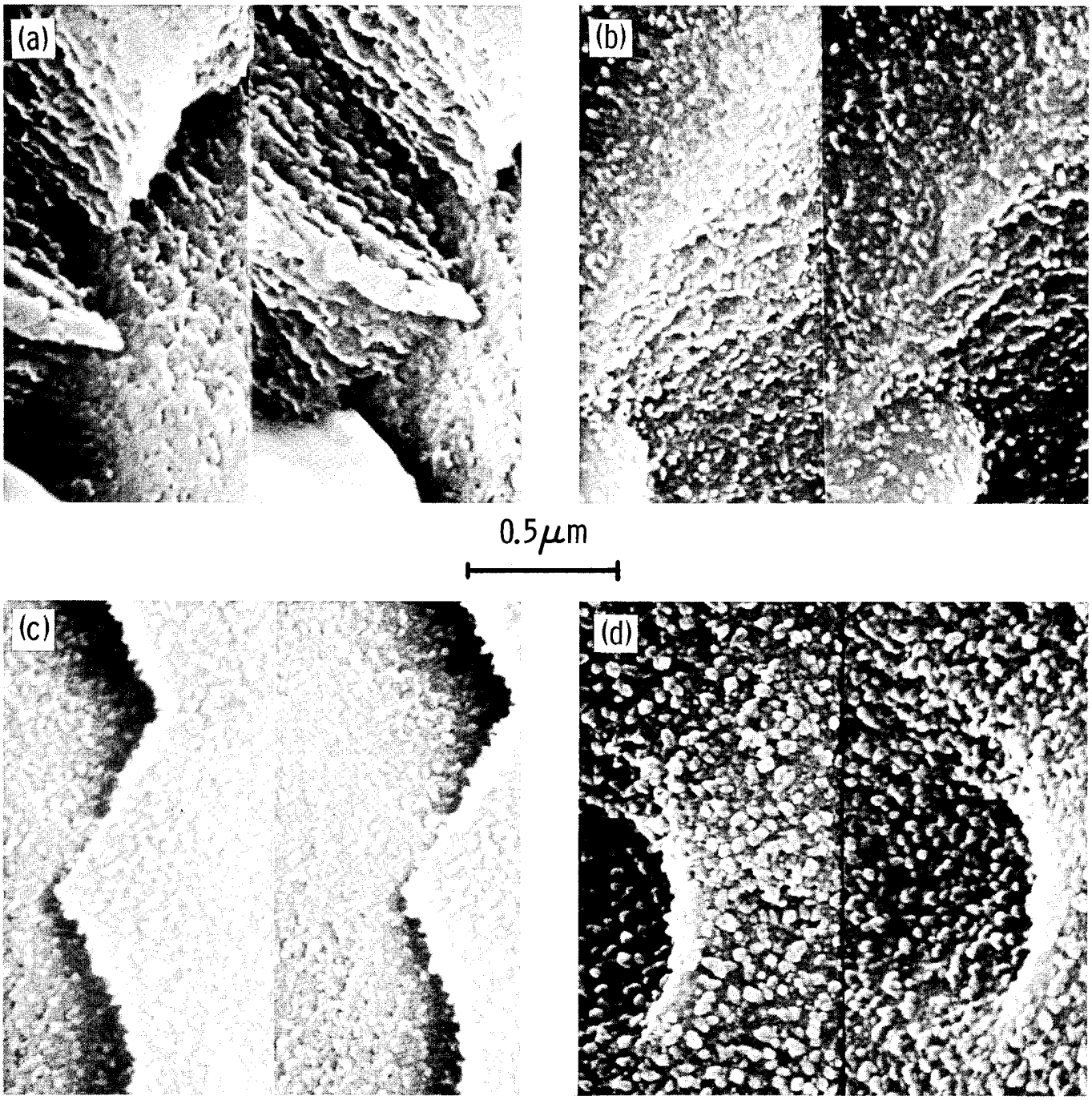

Figure 11. Stereo electron micrographs of surfaces of TU-8-treated Ti-6Al-4V after immersion in 85°C water for (a) 0, (b) 25, (c) 50 and (d) 210 hours.

somewhat porous (Figure 14a). We did not find the rutile structure in our specimen as did Allen et al.[10] After 210 hours, a mixture of polygonal and elongated crystallites covers the whole surface (Figure 13d). They were identified as anatase, although the SAD pattern (Figure 15c) actually is composed of reflections from two and maybe three different structures, the others being cubic TiO and possibly rutile (see Appendix B). The innermost ring corresponds to the strongest anatase reflection {101}, whereas the second ring does not match any TiO_2 reflection, but may belong to the {101} rutile or {111} TiO 8F reflection. However, since the strongest {110} rutile reflection is missing (Appendix B), we cannot conclude that this adherend oxide has a significant rutile phase. This situation raises the possibility that anatase nucleation in water is either preceded by TiO formation, as Fraker and Ruff[20] indicate, or the two occur simultaneously. At 25 hours (Figure 13b), the surface looks practically unchanged, indicating a longer incubation period for AP-9 than for either PF or TU-8. Both increased oxide thickness and stability (the latter due to lack of contamination, especially F) may increase the incubation time and thus account for this observation. At 50 hours (Figure 13c), the crystallite population is still less evolved than that of PF or TU-8. We also see preferential crystallization, especially on regions of fine porosity (Figure 13c-2). It is less on deeply etched areas with arrays of long thin ridges (Figure 13c-1). At 210 hours the original structure "disappears" completely (Figure 13d) and is replaced by the anatase crystallites. Some of these are elongated, up to 1,000-Å long, and better defined than those on either PF or TU-8 (although we have mentioned that long crystallites appear on a few areas of the PF adherend). The disappearance of the original oxide morphology may occur by: 1) the formation of additional oxide (i.e., corrosion) from the substrate and its deposition over the original or 2) the conversion of the amorphous oxide itself into crystalline anatase through either dissolution-precipitation or solid state structural rearrangement. We do not think that significant corrosion of the Ti substrate occurs in pure water at such short times and relatively low temperatures.

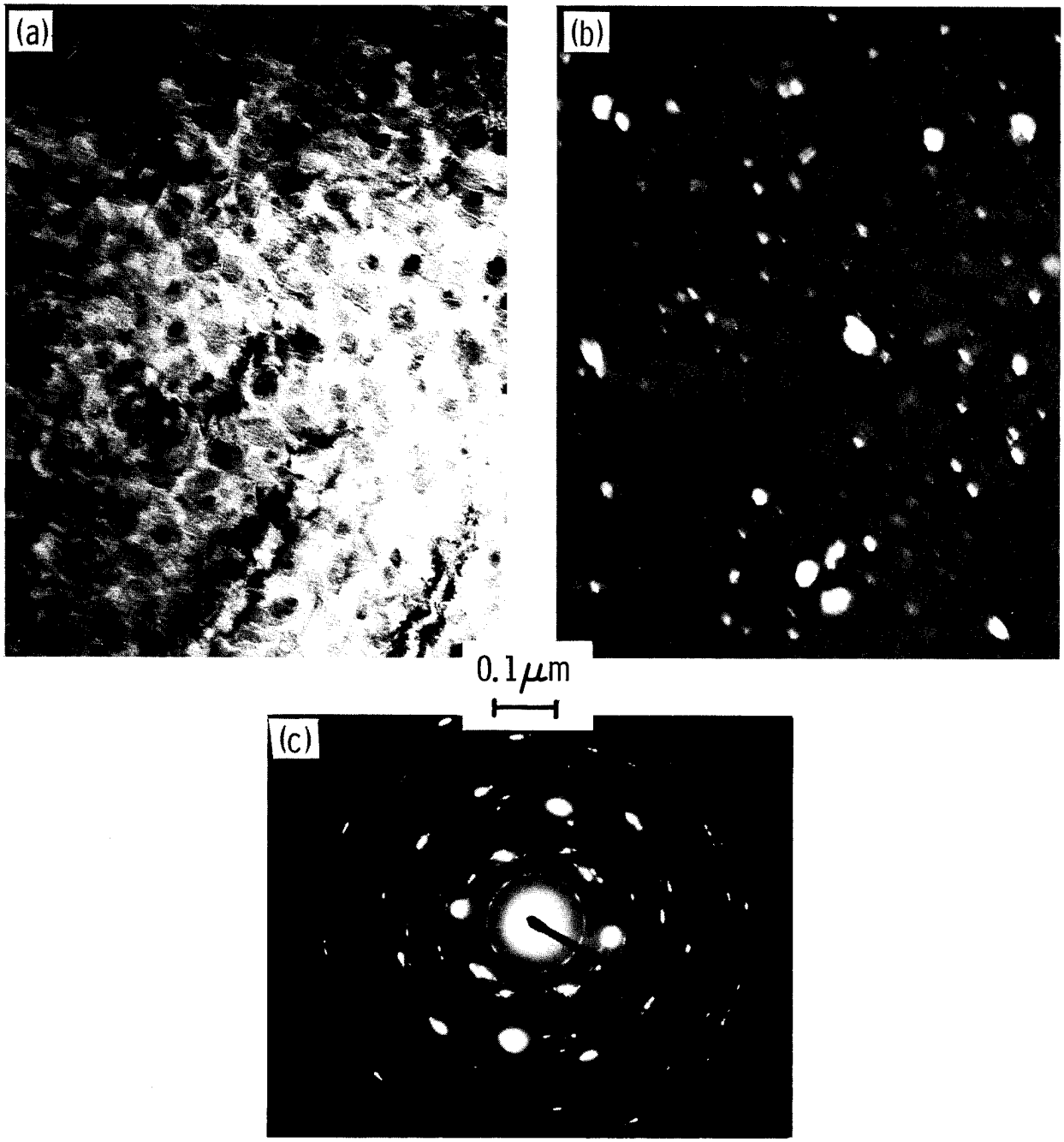

Figure 12. Transmission electron micrographs from the TU-8 oxide after immersion for 210 hours in 85°C in water: a) Bright field, b) Dark field, and c) SAD pattern. The dark-field image was taken from the {101} anatase reflection (innermost ring).

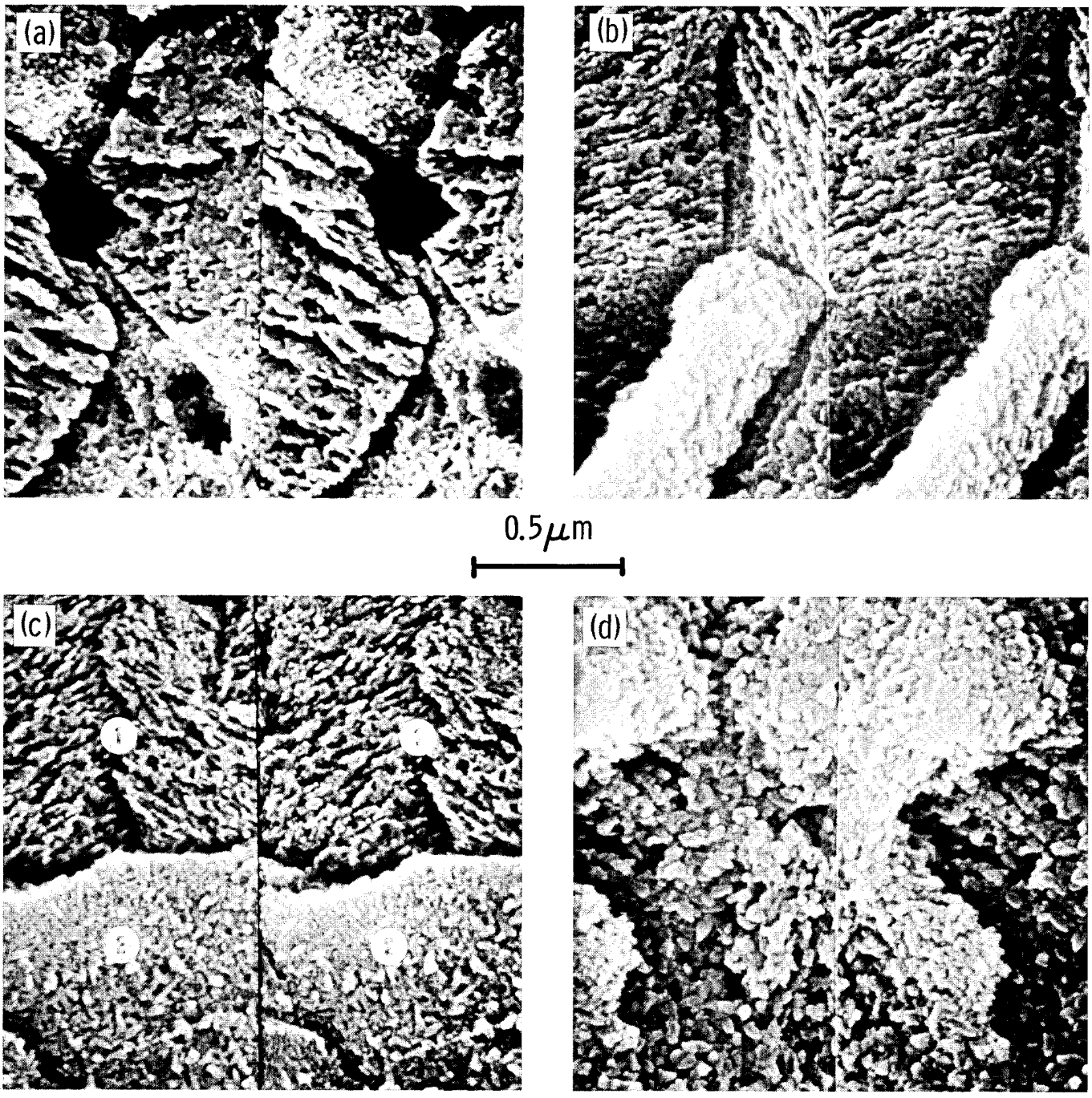

Figure 13. Stereo electron micrographs of surface of AP-9-treated Ti-6Al-4V after immersion in 85°C water for (a) 0, (b) 25, (c) 50, and (d) 210 hours.

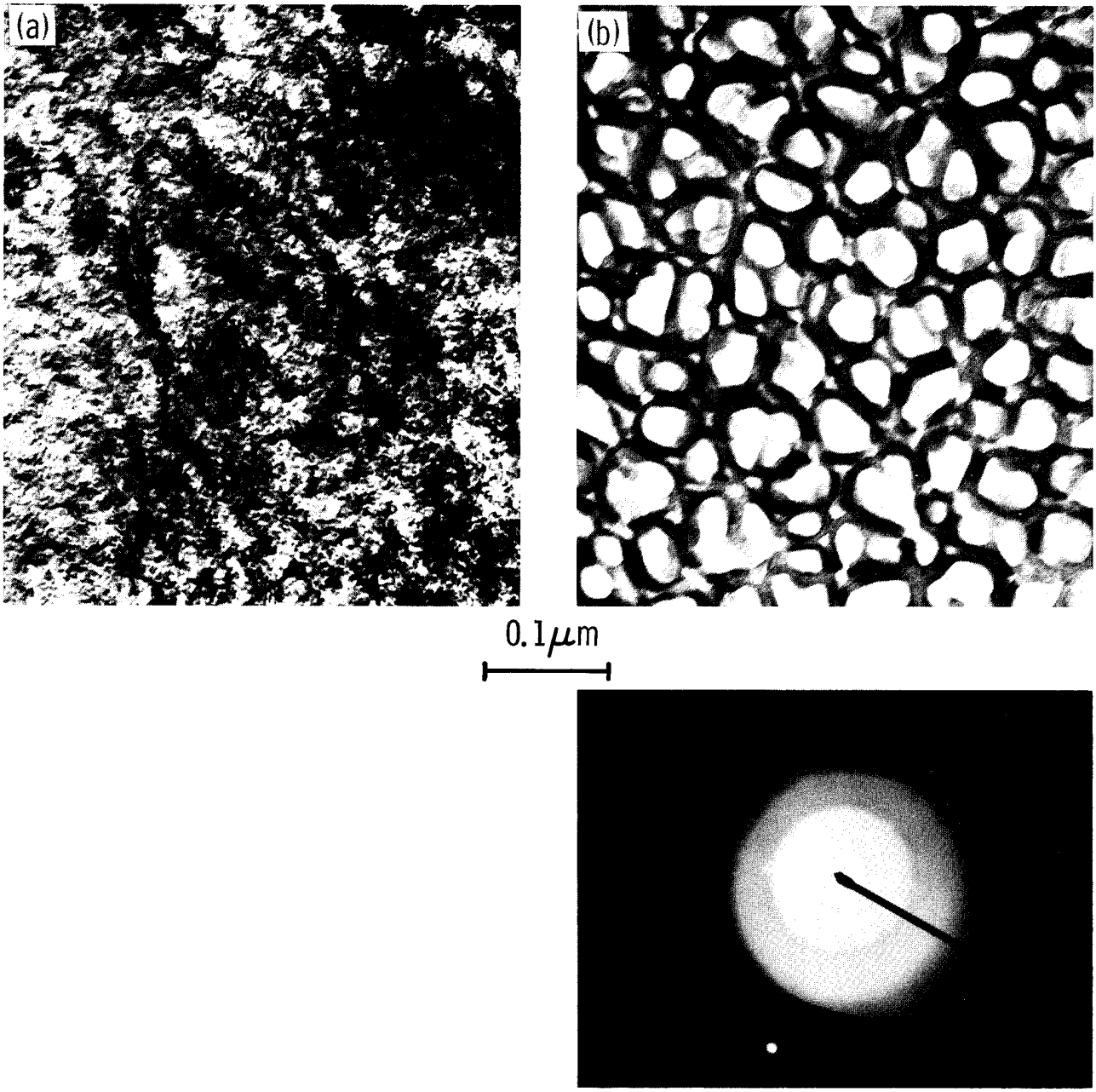

Figure 14. Transmission electron micrographs of a) the AP-9 and b) the CAA oxide prior to water immersion. Both oxides are amorphous.

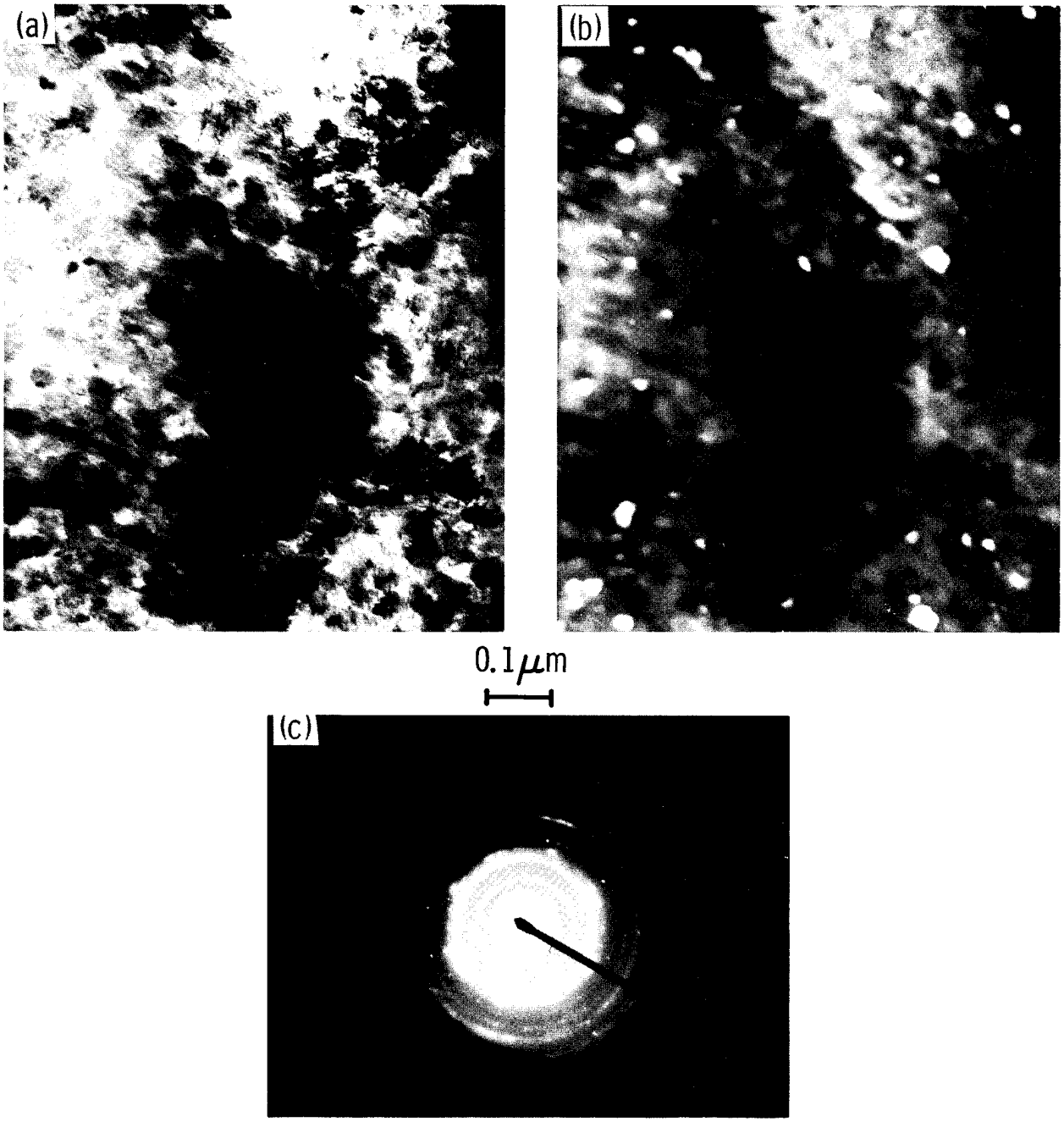

Figure 15. Transmission electron micrographs from the AP-9 oxide after immersion for 210 hours in 85°C water: a) Bright field, b) Dark field, and c) SAD pattern. The dark-field image was taken from the {101} anatase reflection (innermost ring).

4. CAA

This oxide is the thickest of the four, with a well-defined, porous, cellular structure (Figures 14b and 16a). We found that the as-prepared oxide is totally amorphous (Figure 14b). Anodization of a prethinned Ti-6Al-4V foil in a chromic acid bath for TEM specimen preparation yielded the same result.(17) Neither cubic TiO nor crystalline TiO_2 phases were detected anywhere on the original surface. After immersion in water, the oxide undergoes a rapid and dramatic change. Figure 16b shows that by 25 hours the disappearance of the original cells is complete, and the surface is covered with a crystalline layer, identified by SAD as anatase (Figure 17). The crystallites generally are elongated and most sprout rosette-like from a common source outward from the surface. They may eventually become less distinct when additional material, probably from the solution, precipitates between them (arrows, Figure 16d). In the 210-hour, thin-foil sample (Figure 17a), the cell structure is conspicuously absent. Instead, we observe a thin continuous film which contains anatase crystallites of similar size and shape to those viewed with SEM.

This observation suggests that anatase formation involves the disappearance, probably through dissolution in water, of the amorphous TiO_2. Evidence for such dissolution is also seen in Figure 18. Exposure of a CAA-surface to humidity at a lower temperature, 80°C, also results in anatase formation (at a slower rate). However, in these pictures we see an additional feature, namely the appearance, early in the process, of small transparent islands, each of which covers a number of cells, and from which some of the anatase "fingers" grow. In addition, at 72 hours (Figure 18, 3d), some of the cells appear much bigger (arrow), a clear indication of cell-wall dissolution. At 96 hours, most of the original morphology is gone, replaced by the thin-film islands and the anatase fingers. It is possible that the film supporting the anatase crystallites (Figure 17a,b) consists of these thin islands which become continuous after 210 hours. Indeed, the anatase SAD pattern (Figure 17c) contains additional rings which include a weak {200} reflection of cubic TiO. As on the AP-9 surface, anatase formation

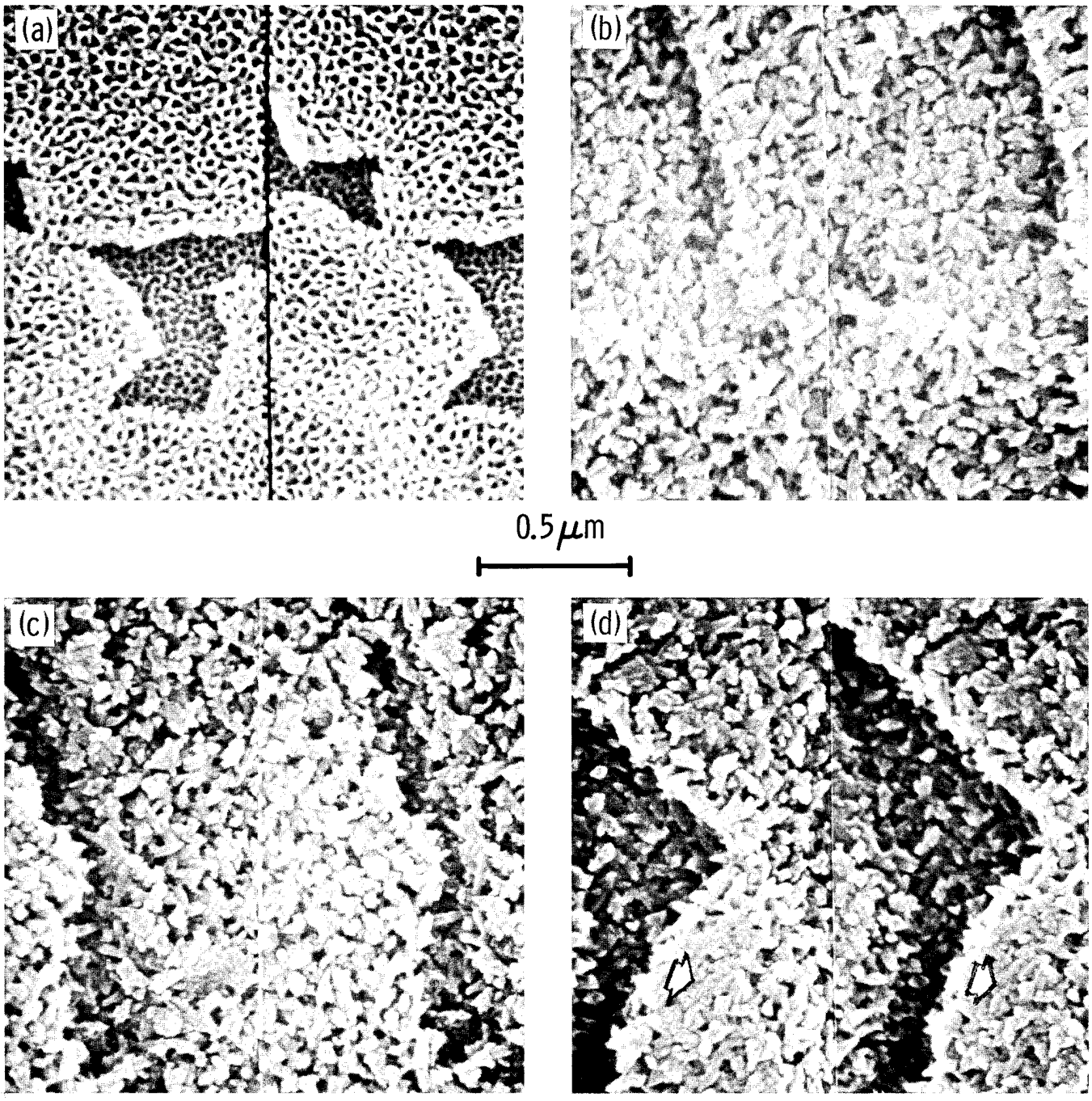

Figure 16. Stereo electron micrographs of surface of CAA-treated Ti-6Al-4V after immersion in 85°C water for (a) 0, (b) 25, (c) 50, and (d) 210 hours.

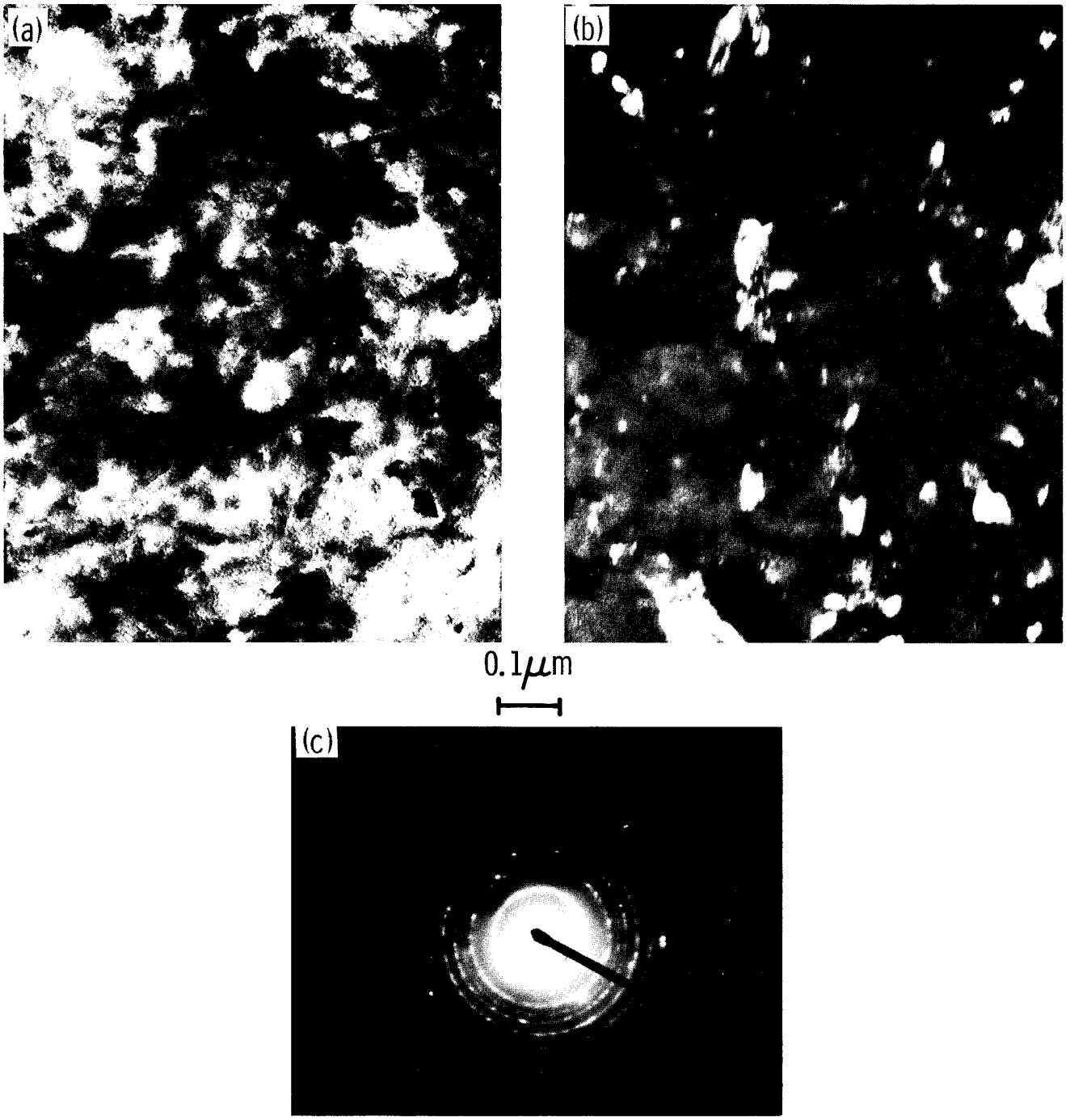

Figure 17. Transmission electron micrographs from the CAA oxide after immersion for 210 hours in 85°C water: a) Bright field, b) Dark field and c) SAD pattern. The dark-field image was taken from the {101} anatase reflection (innermost ring).

is apparently related to the existence of TiO, possibly as a precursor phase.

C. SALT WATER IMMERSION EFFECTS ON Ti ADHERENDS

The effect of salt water on the oxide was checked by immersing a CAA specimen in a 3.5 wt.% NaCl solution. Exposure in a Parr bomb at 140°C and 5 hours yielded results (Figure 19b) very similar to those obtained in pure water (Figure 19a). In both cases, the surface was covered completely with anatase crystallites of equal size ($\leq$ 2500 Å) and shape. However, immersion tests in salt water below 100°C did not result in any changes. It appears that the CAA oxide is more stable in salt water than in pure water at lower temperatures. The reasons for this increased oxide stability are not clear.

D. SUMMARY OF RESULTS

We have described most of the important morphological and structural changes of water-immersed Ti adherends. Following is a summary of the main observations:

a) All four adherends studied have after-treatment oxides which are mainly amorphous. A significant dispersion of cubic TiO microcrystals exists in the PF oxide. Some traces of this phase were also seen in the TU-8 and AP-9 oxides.

b) The exact stoichiometry of the amorphous oxide was not determined; however, it probably is close to TiO_2. This oxide crystallizes into anatase upon exposure to hot water. Rutile, which a number of previous investigators claim exists on water-reacted adherends, was not found on any of our samples.

c) In addition to anatase in the form of small, dispersed crystallites, the presence of cubic TiO on exposed CAA and AP-9 surfaces is indicated by SAD.

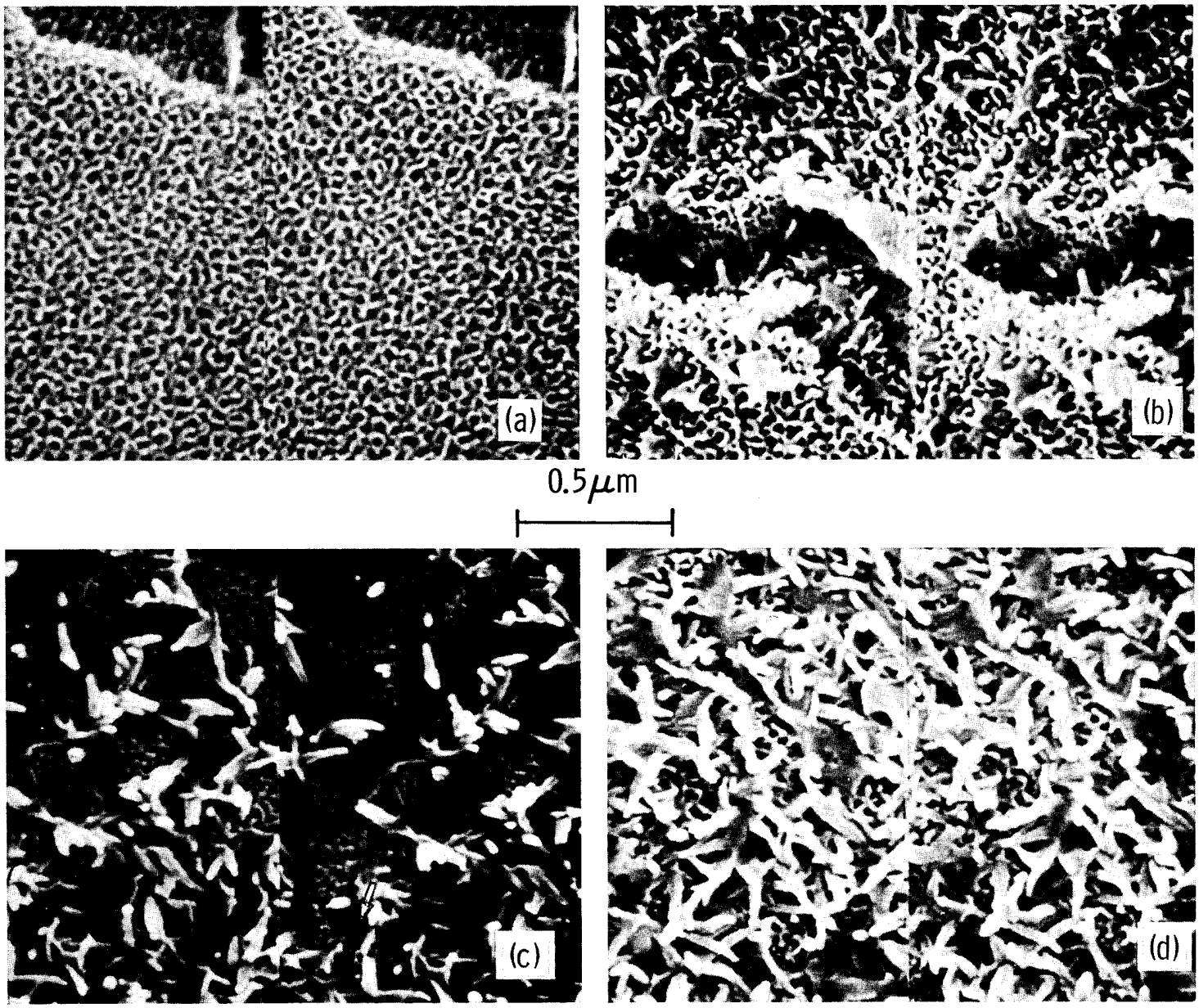

Figure 18. Stereo electron micrographs of surfaces of CAA-treated Ti-6Al-4V after immersion in 80°C water for (a) 0, (b) 1, (c) 3, and (d) 4 days, as indicated.

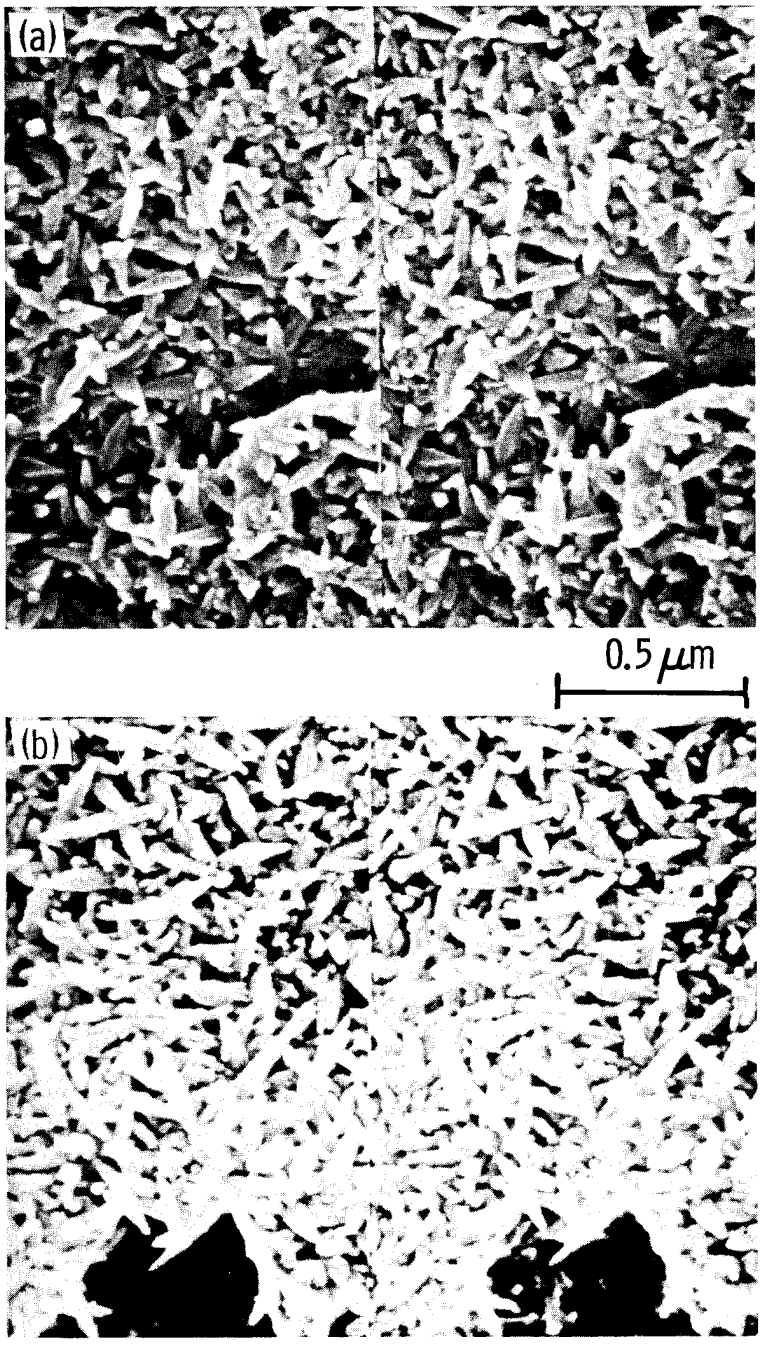

Figure 19. Surfaces of CAA-treated Ti-6Al-4V after 5 hour immersion in 140°C (a) water and (b) 3.5 wt.% NaCl solution.

d) After exposure to hot water, the PF surface becomes only partially covered with anatase crystallites, whereas the coverage of TU-8, CAA, and AP-9 is total.

e) Incubation time for anatase formation is shortest on the most porous and thickest oxide, i.e., CAA. The crystallite growth rate is also fastest on this surface. Both nucleation and growth rate are strongly temperature dependent.

f) Crystallite shape depends on original oxide morphology, temperature, and time. PF, TU-8, and AP-9 surfaces have mostly equidimensional crystallites. On the CAA surface, these are finger-like, longer ($\leq$ 2500 Å), and sharper facetted at high temperatures.

g) Anatase growth on the CAA surface is related to the disappearance of the original oxide cells. At low temperatures, crystallite growth is preceded by the appearance of thin, transparent islands which cover a number of adjacent cells. Diffraction patterns and the literature[20] suggest that these islands may be TiO.

h) Prolonged immersion leads to "dulling" of crystallite shape. This effect is most noticeable on CAA and AP-9 surfaces. Some areas appear to have additional material deposited on the surface after crystallite growth. Such deposition may occur in a dissolution-precipitation process, which could also account for elongated crystallite shape. The two most likely mechanisms of oxide transformation are discussed in the following section.

E. MECHANISMS OF WATER-INDUCED OXIDE TRANSFORMATIONS

Crystallization of the amorphous Ti oxide immersed in water is a complicated subject, but for the sake of simplification we suggest it may occur by one of the following mechanisms: 1) structural rearrangement and

epitaxial growth of the crystalline phase or 2) dissolution of the amorphous oxide and precipitation of the new crystalline phase from the now supersaturated solution. Either mechanism may be accompanied by oxidation of Ti released from the substrate, i.e., corrosion. Evidence that would distinguish between these mechanisms is scarce, although a number of papers have dealt with the subject in connection with the hydrothermal crystallization of anatase and rutile in aqueous solutions.(16,21,22) Matthews(16) proposes a mechanism of anatase crystallization from a reactive starting material (amorphous TiO_2 or titanic acid) through spontaneous nucleation and successive epitaxial growth processes. He assumes that nucleation occurs in regions of the reactant where short-range order, analogous in structure to anatase, already exists. The crystals that grow by this process are apt to be equidimensional and should not show sharp, crystallographic facets. On the other hand, as Izumi(22) noted, the dissolution-precipitation mechanism will create polygonal microcrystals with smooth surfaces. Crystallites nucleate spontaneously due to a high local supersaturation of the solution and grow by transfer of material from the reactant.

We can make a number of strong arguments against the ability of the structural rearrangement mechanism to account for the observed anatase fingers, especially on the CAA surface. For a finger to grow out of a planar, amorphous layer, there first should be local crystallization followed by outward growth through diffusion, either in the bulk or on the finger surface. Disregarding the exact nature of the diffusing species (both Ti and O are needed to form anatase), formation of the finger shape probably requires the fastest process, i.e., surface diffusion. However, this choice is thermodynamically impossible, since it implies atom migration <u>up</u> a chemical potential gradient. In the absence of an external driving force for diffusion, surface migration will always occur from the finger tip to its base, since the chemical potential at the tip is higher, due to the small radius of curvature.(23) As for

---

22 F. Izumi, ibid, <u>51</u>(6) (1978), 1771-1776.
23 P.G. Shewmon, Diffusion in Solids, McGraw-Hill Book Co., Inc., New York (1963).

local crystallization at the finger base, which is a prerequisite, a recent study by Shiojiri et al.[24] implies that it would be rather slow under 100°C. Crystallization of a 400-Å-thick TiO_2 layer, defined as the appearance of 100-300-Å-wide crystalline regions, required 1 hour at 500°C in vacuum. For a much thinner film (100 Å), at 450°C, regions of 20-30 Å took 4 hours to develop, and 100-300 Å took 12 hours. Even allowing for a somewhat faster crystallization in an 800 Å film (as on CAA), the time required for the development of 300-400-Å-thick fingers will probably be an order of magnitude greater, in contrast to our observations. Therefore, we conclude that this mechanism may partially account for the original nucleation of the anatase phase, but not for the subsequent growth.

The dissolution-precipitation mechanism, on the other hand, is clearly favored thermodynamically and requires the presence of the water medium. The driving force is provided by the lowering of the free energy of the oxide in the transformation from a metastable amorphous state to a stable crystalline one[13,24] and by the external heat. Moreover, our observations on the amorphous TiO_2 - anatase transformation on CAA surfaces tend to support a dissolution-precipitation mechanism and suggest the following sequence of events:

When amorphous TiO_2 is dissolved, some Ti and O ions from the solution may precipitate as TiO, possibly on pre-existing TiO nuclei. Eventually, oxygen supersaturation develops. Anatase nuclei may then develop through TiO oxidation and/or direct structural rearrangement of the amorphous phase. Growth occurs through further precipitation governed by surface energy.

The speed of nucleation and growth of anatase on the cellular CAA oxide vs other adherends is probably due to increased localized acidity and supersaturation in the cells. Increased acidity due to release of F contaminant ions into the small volume of solution in each pore is highly probable (Appendix C). The situation is analogous to the increased acidity

---

24 M. Shiojiri, T. Miyano and C. Kaito, Japan J. Appl. Phys. 18(10) (1979), 1937-1945.

at the crack tip in stress corrosion cracking[25] or crevice corrosion.[26] In both cases, the local acidity can be much higher than that of the solution, which itself may be neutral or even alkaline. Increased acidity due to F may lead to increased dissolution of the Ti (IV) oxide.[22] Local supersaturation inside the small pores may be reached quickly and lead to precipitation of anatase, not rutile, since anatase has a lower surface energy than rutile.[16] Anatase probably dissolves less in the acidic medium than amorphous TiO_2. The behavior of other Ti adherends will depend on the surface contamination and porosity. Non-porous oxides (as on PF and TU-8) will probably create non-localized and much weaker acidic conditions even if F is present on the surface. The more porous AP-9 oxide is free of F contamination. Therefore, the localized solution acidity is probably weaker than that on CAA or PF.

The results on other surfaces do not contradict the dissolution-precipitation mechanisms proposed for CAA. On PF, the original oxide is so thin that we would not expect crystallites growing by structural rearrangement to be much longer than 100 Å. However, some areas on the surface exhibit anatase fingers 1000-Å long, while others are anatase free. This is a strong indication that material was transported to the growing finger from elsewhere on the surface. Epitaxial relationships may be important in the nucleation stage and, as already mentioned, may help anatase nucleation on the cubic TiO phase.

F. SURFACE CHANGES AND ADHESIVE BOND FAILURE

In our earlier study[17] we showed that bond durability in Ti adherends mainly depends on its mechanical component. Group III adherends (CAA,AP) have very durable bonds since their rough, porous oxides provide good mechanical interlocking with the primer. Durability decreases with

---

25 B.F. Brown, C.T. Fujii and E.P. Dahlberg, J. Electrochem. Soc. 116(2) (1969), 218-221.

26 J.C. Gries, Corrosion 24(4) (1968), 96-109.

decreasing oxide microroughness, being smallest in Group I (PF,MPF) adherends. Thus, it was shown that in wedge tests at 140°F and 100% R.H., Group I adherends (PF,MPF) failed adhesively; in Group II, DP-2 and DA-5 failed adhesively, TU-8 in a mixed adhesive-cohesive mode, and LP-6 cohesively. From Group III, the only tested adherend, CA10-4, failed cohesively in the adhesive. In two lap shear tests on MPF and LP-6 adherends at 140°F and 100% R.H., the MPF specimen failed adhesively as did (in contrast to the wedge test result) the LP-6 specimen. The adherend-side morphologies of all failed surfaces except one were similar to those of prebonded, as-prepared specimens. The exception was the failed MPF lap shear specimen. Its surface on the Ti side is shown in Figure 20. It does not display any of the ridges typical of an MPF surface; rather it exhibits a fine structure which resembles the anatase crystallites on the PF surface at a very early water immersion stage. These structures appear in a few small areas on the surface and were too small to be chemically analyzed with Auger/ESCA techniques.(17) The crack that propagates at the interface between these features and the primer is possibly related to a structural weakening due to an oxide transformation.

The process of immersion of a free adherend-oxide surface in water may not be analogous to permeation of water into the oxide-primer interface. Likewise, in the adhesively bonded structure, the humid atmosphere at the tip of an advancing crack may resemble only remotely the solution in an immersed oxide pore. These differences may result in much slower kinetics of oxide transformation and possibly an increase in the relative importance of structural rearrangement and epitaxial growth vs. dissolution-precipitation. Although the transformation will be restricted and slower, it may still affect the bond through increased stresses induced by the new growing phase.

We lack information on crystal structure of the failed wedge and lap shear surfaces, and particularly of the CAA adherend. We plan to continue our investigations of this type of adherend, since it shows the best durability and bond strength of all adherends tested so far. Moreover,

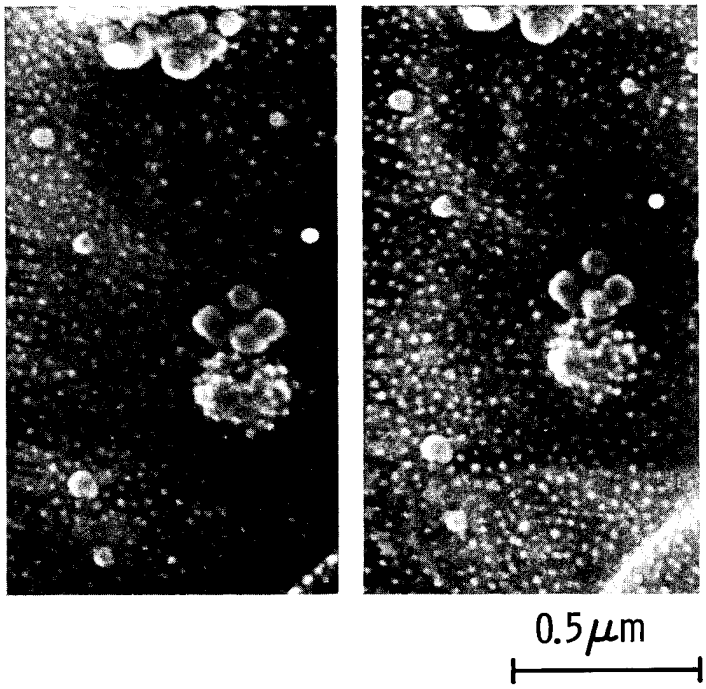

Figure 20. Stereo electron micrograph of the surface of a MPF lap shear specimen which had failed adhesively when loaded for 61.2 hr at 800 psi in a 140°F, 100% R.H. environment.

crystal structure studies of failed wedge and lap shear test specimens are needed to determine whether failure is induced by an oxide phase transformation. If such a transformation occurs, we would intend to study the crystallization of amorphous TiO_2 into anatase, without affecting the original morphology, in the hope of improving bond durability.

IV. CONCLUSIONS

A. ADHEREND CHARACTERIZATION

PF-3 - We classify PF-3 as a Group I adherend by its morphology. Its oxide has a thickness of ~ 100 Å and is contaminated with F and Cu. Bondability should be similar to that of other PF adherends.

VA-7 - We assign this adherend to Group I and expect its bondability to be very similar to that of PF. The surface oxide has Si and Al contamination, probably from the forming slurry, but no fluorine.

AP-9 This commercially prepared adherend is classified as belonging to Group III. It has an oxide thickness of ~ 550 Å, and it is free of contamination. It is only half as thick as, and less porous than, an AP adherend prepared at Martin Marietta Laboratories, which suggests variability in this process. Its bondability should be better than that of most other adherends and comparable to that of CA10-4. More studies are needed to determine the source of the observed variability in oxide morphology and the effect this has upon bond strength and durability.

B. HOT WATER IMMERSION STUDIES

- Four adherends -- PF, TU-8, CAA, and AP-9 -- were tested in a hot water environment. All were characterized structurally prior to testing and found to have a surface oxide that was mainly amorphous TiO_2. In addition, PF had a dispersed phase of small cubic TiO crystallites, traces of which were also detected in TU-8 and AP-9 oxides by SAD.

- Upon immersion in hot water, the amorphous TiO_2 crystallizes into anatase in the form of small (100-2500Å) anatase crystals dispersed

over the adherend surface. No rutile crystals existed at the end of our runs on any of the adherends tested.

- Anatase formation is influenced by original oxide morphology, contamination, thickness, porosity, and water temperature.

- Evidence is presented which supports a dissolution-precipitation mechanism for the observed oxide transformation. In some cases, anatase nucleation may occur on an existing TiO phase.

- Only one lap shear test shows adherend morphology changes similar to those observed in the immersion tests. However, we cannot discount the possibility that crystallization of the amorphous oxides without a morphology change may occur under certain conditions, and bond durability might be affected by this change. Further work is needed in this area.

- The results suggest that bondability of CAA and AP adherends might be improved by pre-crystallizing the amorphous oxide into anatase, without changing the original morphology. This treatment would inhibit dissolution of the oxide and stabilize it against further changes.

APPENDIX A

A. Code for Ti adherend pretreatment processes

PF	Phosphate fluoride	LP	Liquid hone/PASA Jell
CA	Chromic acid anodization	TU	Turco 5578
PA	Phosphoric acid anodization	DA	Dapcotreat 4023/4000
DH	Dry hone	VA	VAST
DP	Dry hone/PASA Jell	AP	Alkaline peroxide

B. Phosphate fluoride (PF) and chromic-acid-anodization (CAA) treatments as performed at Martin Marietta Laboratories.

1. PF

a. Vapor degrease Ti-6Al-4V coupon by hanging specimen over boiling trichloroethylene for 10 minutes.

b. Pickle at room temperature for 30 seconds in a solution of 15 vol% of 70% HNO_3 and 3 vol% of 49% HF.

c. Rinse twice in distilled deionized water; a 2-minute immersion each time.

d. Treatment

Immerse for two minutes at room temperature in a mixture of:

Trisodium phosphate	50 g/l solution
Potassium fluoride	20 g/l solution
HF 50%	26 ml/l solution

e. Rinse - repeat step c.

f. Soak in 65°C tap water for 15 minutes.

g. Rinse - repeat step c.

h. Blow dry.

2. CAA

a. Degrease, pickle, and rinse as in steps a-c above.

b. Anodize for 20 minutes at room temperature in a solution of 5 wt% chromic acid and 1 g/l solution of NH_4F at 10 V and at a current density of 0.002 A/cm^2.

c. Rinse, soak, and blow dry as in steps e-h above.

APPENDIX B

The indexing of a SAD pattern may be performed in two ways:

A. If the camera constant $L\lambda$ is known, we measure the radius, R, of the ring corresponding to a $\{hkl\}$ reflection and calculate the spacing d_{hkl} from:

$$d_{hkl} = \frac{L\lambda}{R} \quad . \tag{1}$$

B. If $L\lambda$ is not known, we use the Ratio Method which is based on Eq. (1)

$$\frac{d_1}{d_2} = \frac{R_2}{R_1} \quad . \tag{2}$$

Our camera constant was calibrated from a standard, poly-crystalline Al specimen and was found equal to $(5.45 \pm 0.05) \times 10^8$ Å2. All patterns could therefore be indexed by method A and checked by method B.

Table I shows the indexing of the patterns in Figure 9a. Table II shows that even with a much bigger error in $L\lambda$ than our ± 1%, the pattern in 9a could not be mistaken for rutile or anatase. The indexing of all anatase patterns was also done by method A and periodically checked with the ratio method. Table III is another example of the indexing method using the pattern in Figure 17c.

C. Rutile vs anatase -- We took special care to differentiate between rutile and anatase patterns. Our conclusion that no significant rutile phase exists on immersed oxides is based mainly on the absence of the strongest rutile reflection {110} from all of our patterns. This reflection should give rise to rings or dots located on a diameter, D = 1.68 cm. Other strong rutile reflections should appear as rings or dots with diameters of 2.19 cm ({101}) and 3.23 cm ({211}) (camera constant taken at the average value of 5.47×10^8 Å2). However, these can be confused with the {111} (TiO) 8F and {105} anatase reflections.

Table I. Indexing of the SAD pattern in Figure 9a. Camera constant = 5.4 x 108 Å2.

PF			(TiO)8F	
Ring Diameter (cm)	d_{hkl} (Å)	Intensity	d_{hkl} (Å)	Intensity I/I_1
2.20	2.45	Strong Diffuse	2.407	45
2.57	2.10	Strong	2.085	100
3.65	1.48	Strong	1.475	50
4.26	1.27	Very weak	1.259	13
4.45	1.21	Medium	1.205	12
5.16	1.05	Weak	1.044	5
5.83	0.93	Medium	0.934	13
6.39	0.85	Medium	0.852	14

Table II. Comparison of R_1/R_2 values, where R_2 is the radius of the second smallest ring in the SAD pattern. Only rings of $I/I_1 > 10$ are considered. The PF pattern is that of Figure 9a.

$PF_{original}$	(TiO)8F	Rutile	Anatase
0.85	0.866	0.765	0.69
1.00	1.00	1.00	1.00
1.42	1.413	1.136	1.022
1.66	1.656	1.210	1.042
1.75	1.730	1.474	1.284
2.02	1.997	1.531	1.430
2.28	2.232	1.660	1.459
2.51	2.447	1.711	1.641

Table III. Indexing of the SAD pattern in Figure 17c. The crystal structure is anatase. The third ring (d = 2.06) probably consists of the strong, cubic TiO {200} reflections. Camera constant = 5.47 x 108 Å2.

SAD Pattern			Anatase		(TiO)8F	
Ring diameter (cm)	d_{hkl} (Å)	Intensity	d_{hkl} (Å)	Intensity I/I_1	d_{hkl} (Å)	Intensity I/I_1
1.56	3.52	Strong	3.52	100		
2.33	2.39	Medium-strong	2.378 2.332	20 10	2.407	45
2.65	2.08	Weak			2.085	100
2.90	1.92	Medium	1.892	35		
3.29	1.69	Medium-strong	1.70 1.666	20		
3.74	1.49	Medium-strong	1.481	14	1.475	50
4.09	1.36	Weak	1.337	6		
4.38	1.27	Weak	1.265	10	1.259	13
4.74	1.17	Weak	1.166	6	1.205	12
5.27	1.05	Weak	1.051	4	1.044	5
5.51	1.01	Very weak	1.007	2	0.958	5
5.80	0.96	Very weak	0.955	4	0.934	13

APPENDIX C

Concentration of F^- ions in a typical CAA oxide pore

We assume that there is a 6% monolayer of F atoms covering the inside wall of a round pore which has a diameter of 600 Å and a height of 800 Å. If the pore is filled with water and all the F^- ions of the first monolayer are dissolved, we have:

1. Atoms/cm^2 pore wall = (Avogadro's number)$^{2/3}$ = 3.3×10^{16} atoms/cm^2
2. Moles/cm^2 pore wall = $3.3 \times 10^{16}/6.022 \times 10^{23}$ = 5.479×10^{-8} moles/cm^2
3. Pore volume = $\pi r^2 h = 2.262 \times 10^{-16}$ cm^3
4. Pore area = $2\pi rh = 1.508 \times 10^{-10}$ cm^2
5. Moles/pore = $(5.479 \times 10^{-8}) \times (1.508 \times 10^{-10})$ = 8.262×10^{-18} moles/pore
6. Moles F/pore = $0.06 \times 8.262 \times 10^{-18}$ = 4.957×10^{-19} moles F/pore

Molar F^- concentration =

$$\frac{4.957 \times 10^{-19}}{2.262 \times 10^{-16}} = 2.2 \times 10^{-3} \text{ moles F/cm}^3$$

equivalent to 2.2 M HF

REFERENCES

1. B.M. Ditchek, K.R. Breen, T.S. Sun, J.D. Venables and S.R. Brown, 12th Nat. SAMPE Tech. Conf., Seattle, WA (1980), p. 882.
2. A.C. Fraker and A.W. Ruff, Jr., Corros. Sci. 11 (1971), 763-5.
3. W.C. Hamilton, G.A. Lyerly and J. Fronhsdorf, Technical Report 4362, 6/1972, Gillette Research Institute, Rockville, MD.
4. A.A. Roche, Technical Report AFWAL-TR-80-4004, Feb. 1980.
5. G.W. Lively, Technical Report AFML-TR-73-270, Jan. 1974.
6. A.A. Roche, J.S. Solomon and W.L. Baun, Appl. Surf. Sci. 7 (1981), 83-96.
7. J.M. Abd El Kader, F.M. Abd El Wahad, H.A. El Shayeb and M.G.A. Khedr, Br. Corros. J. 16(2) (1981), 111-114.
8. F. Dalard, C. Montella and J. Gandon, Surf. Technol. 8 (1979), 203-224.
9. G. Blondeau, M. Froelicher, M. Froment and A. Hugot-LeGoff, Proc. 7th Int. Vac. Congr. and 3rd Int. Conf. Solid Surf., Vienna (1977), 1789-1791.
10. K.W. Allen, H.S. Alsalim and W.C. Wake, J. Adhes. 6 (1974), 153-164.
11. A. Polity, G. Jouve and P. Lacombe, J. Less-Common Met. 56 (1977), 263-268.
12. T. Smith and D.H. Kaelbe, Technical Report AFML-TR-74-73, June 1974.
13. K.H. Behrndt, J. Vac. Sci. Technol. 7(3) (1969), 385-398.
14. J.D. Venables, D.K. McNamara, J.M. Chen, B.M. Ditchek, T.I. Morgenthaler, T.S. Sun and R.L. Hopping, 12th Nat. SAMPE Tech. Conf., Seattle, WA, (1980), p. 909.
15. J.S. Ahearn, private communication.
16. A. Matthews, Am. Mineral. 61 (1976), 419-424.
17. B.M. Ditchek, K.R. Breen and J.D. Venables, MML TR-80-17c, Final Report to NAVAIRSYSCOM, Contract #N00019-79-C-0294 (1980).
18. R. Siriwardane and J.P. Wightman, Final Report NASA-CR-162903, March 1980.
19. W. Chen, D.W. Dwight and J.P. Wightman, Symposium on Surface Analysis, Pittsburgh Conf. on Analytical Chem. and Appl. Spectrosc., Cleveland, OH, May 12-16, 1978.
20. A.C. Fraker and A.W. Ruff, Titanium Sci. Technol., Proc. Int. Conf., 2nd, 4 (1973), 2655-63.
21. F. Izumi and Y. Fujiki, Bull. Chem. Soc. Japan 49(3) (1976), 709-712.
22. F. Izumi, ibid, 51(6) (1978), 1771-1776.
23. P.G. Shewmon, Diffusion in Solids, McGraw-Hill Book Co., Inc., New York (1963).
24. M. Shiojiri, T. Miyano and C. Kaito, Japan J. Appl. Phys. 18(10) (1979), 1937-1945.
25. B.F. Brown, C.T. Fujii and E.P. Dahlberg, J. Electrochem. Soc. 116(2) (1969), 218-221.
26. J.C Gries, Corrosion 24(4) (1968), 96-109.

BONDABILITY OF Ti ADHERENDS

Performing Organization: Martin Marietta Laboratories

Objective of Study

1. To determine surface morphology and surface chemistry of Ti adherends produced by different (9) pretreatments

2. To correlate above findings with wedge and lap shear test results performed by Brown and Wegman, respectively

3. To determine morphological and structural changes in adherend surfaces exposed to humidity

4. To suggest changes in existing processes or develop new ones for improved bondability

Conclusions - Morphology

1. The PF and MPF and VA processes produce thin oxides with little micro- or macro-roughness and low bond strength

2. The DA, DP, LP, and TU processes yield thin, macro-rough oxides that produce intermediate to high bond strength, depending on the degree of micro-roughness. Within this group, TU exhibits the most micro-roughness and best mechanical properties.

3. The CAA process yields thick porous oxides. Bond strength is therefore high.

4. The AP morphology varies considerably depending upon treatment parameters. Our current work demonstrates that rough porous oxides can be generated by modifying the commercial treatment.

5. The bond strength in thick and porous oxides is derived mainly from mechanical interlocking between oxide "fingers" and cells, and the adhesive.

Conclusions - Humidity Effects

1. The oxides formed on Ti by the PF, TU, CAA, and AP processes are mainly amorphous and have roughly a TiO_2 composition.

2. Upon immersion in hot water, the amorphous TiO_2 crystallizes into anatase. No rutile was found in our experiments.

3. Crystallization is influenced by the original morphology (thickness, porosity), contamination, and water temperature.

4. The crystallization process probably involves the dissolution of the amorphous phase in water and the precipitation of anatase crystallites.

5. Based on these results, we are investigating the possibility of crystallizing the oxide prior to bonding in order to improve the durability of Ti bondments.

Tools and Techniques

1. Scanning transmission electron microscopy (STEM) in high resolution SEM, transmission, and selected area diffraction (SAD) modes

2. Auger electron spectroscopy

3. X-ray photoelectron spectroscopy (XPS)

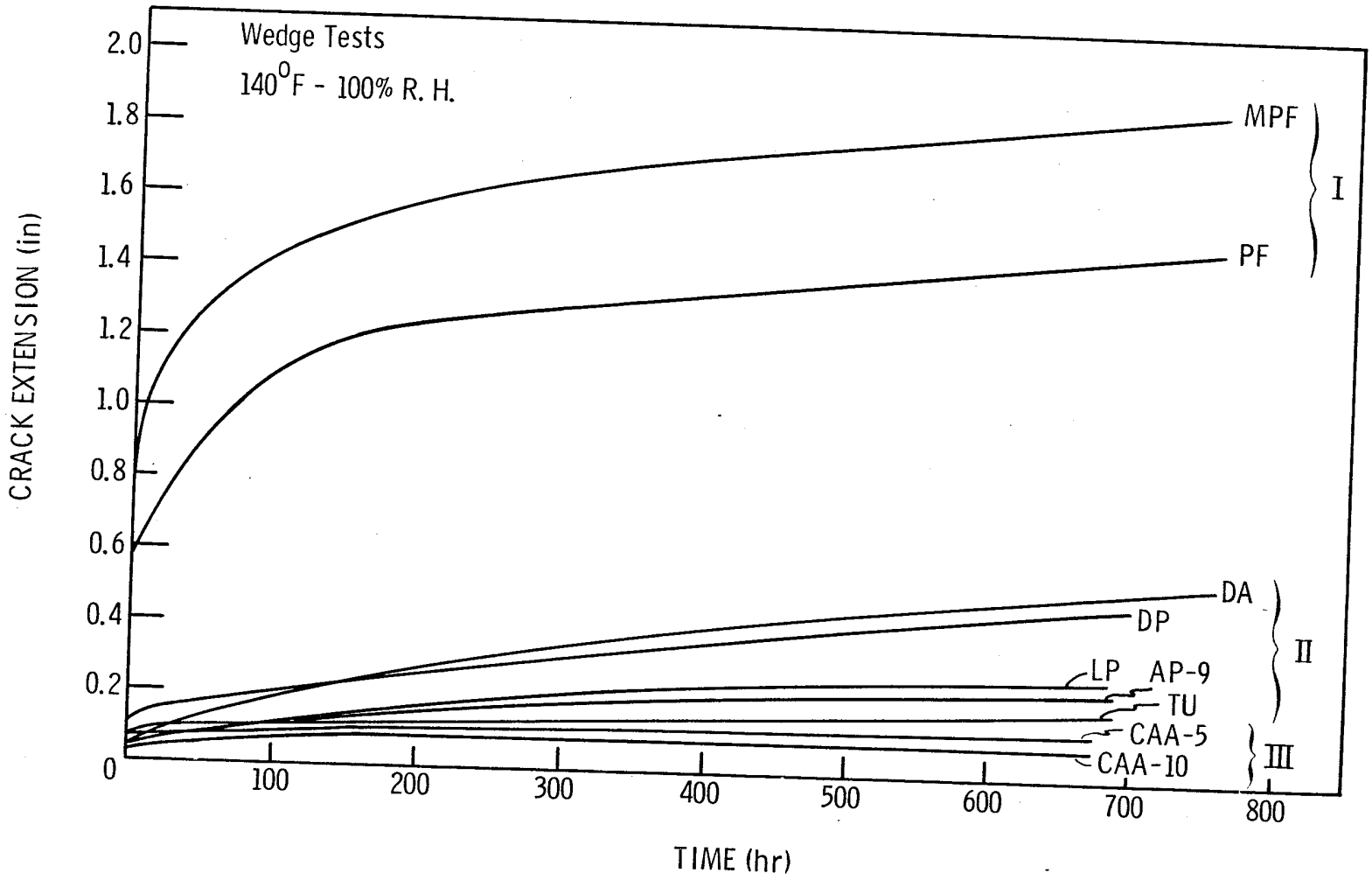
Wedge Tests
140°F - 100% R. H.
CRACK EXTENSION (in)
2.0
1.8
1.6
1.4
1.2
1.0
0.8
0.6
0.4
0.2
0
100
200
300
400
500
600
700
800
TIME (hr)
MPF
PF
I
DA
DP
LP
AP-9
TU
CAA-5
CAA-10
II
III